
PEREGRINE PARCEL

FINAL REPORT
APRIL 30, 2016
MEAM 445/446
TEAM 14: PEREGRINE
PEREGRINE.PARCEL@GMAIL.COM

ANNA L. BRILL
anbrill@seas.upenn.edu

ALISSA C. JOHNSON
aljo@seas.upenn.edu

WILLIAM R. JOHNSON III
wj@seas.upenn.edu

BENJAMIN T. KRAMER
krab@seas.upenn.edu

RACHEL L. RUSONIS
rusionis@seas.upenn.edu

C. CAMERON ZAWACKI
czawacki@seas.upenn.edu

PRIMARY FACULTY ADVISER

DR. MARK YIM
yim@grasp.upenn.edu

TECHNICAL ADVISER

DR. PAUL POUNDS
paul.pounds@uq.edu.au

CORPORATE LIAISON

DR. NICHOLAS STAPP
nstapp@hersheys.com

SEPTEMBER 2016 - APRIL 2017

<i>CONTENTS</i>	1
-----------------	---

Contents

1 Abstract	6
2 Executive Summary	7
3 Statement of Roles and External Contributions	9
4 Background	11
5 Objectives	16
6 Design and Realization	20
7 Validation and Testing	49
8 Discussion	63
9 Budget, Donations, and Resources	65
A Appendix	68

List of Figures

1	The OXcopter	7
2	Staircase in the Pennovation Center	11
3	The TUG robot in a hospital	13
4	The Relay robot being loaded for hotel delivery	14
5	The Mailmobile automatic delivery system	14
6	Festo's drone delivering a small item [10].	15
7	Amazon Air Drone	16
8	Multirotor Effective Rotor Area	22
9	Triangular quadrotor maneuvering controls.	23
10	Motivation for the OXcopter	25
11	A commercially available contra-rotating motor for smaller flight vehicles	27
12	A commercially available rotor head for an RC helicopter	31
13	The bevel gear propeller clamp system during thrust testing.	31
14	Renderings of structural components designed and machined in the first prototype of the OX subassembly.	32
15	A rendering of the first prototype of the OX subsystem, with labeled components.	33
16	The initial design of the contra-rotating system, with a rotating shaft.	34
17	Bending failure of the first prototype.	35
18	Final flight vehicle, assembled.	36
19	An off-the-shelf shaft collar, used to mount the upper motor and fix the rod to the vehicle.	36
20	A photograph of angled wedges on the wedge adapter.	37
21	A labeled rendering of the final design for the OX subassembly.	37
22	The final design of the contra-rotating system mounted on the thrust stand.	38
23	The quadrotor subsystem, assembled.	39

24 Pictured to the left is the vending machine prototype, and to the right is the final vending machine with OXcopter. 41

25 Software architecture for vehicle missions. 42

26 A Rendering of the OXcopter with the safety system 46

27 A rendering of a lower safety hoop surrounding one of the quadrotor propellers. 47

28 The envisioned steps in our automated delivery system. Scope of the project is highlighted in green. 49

29 Antigravity 4004 motor and twisted blade 50

30 The quadrotor can provide more than enough thrust to lift its own weight of 824g 51

31 Single rectangular blade test setup 52

32 Measurement of the blade pitch angle using LoggerPro 53

33 Single twisted blade test setup 54

34 Single rotor in free air 54

35 Single blade noise results 55

36 The coaxial rotor system had to be supported on the other end 56

37 Noise comparison 57

38 RPM and thrust comparison for single and double twisted blades 57

39 Double twisted blade thrust results 58

40 Double twisted blade torque results 58

41 Thrust and power advantages of coaxial rotors 59

42 Team Peregrine prepares for a hover test 60

43 LiDAR testing setup 61

44 SLAM Validation 62

45 The ramps of the vending machine guide candy into the winch-actuated carriage 63

46 A stadium is an example of a chaotic environment 68

47 An airport is an example of a chaotic environment 69

48 A convention hall is an example of a chaotic environment 69

49	A factory is an example of a chaotic environment	70
50	ADA doorway standards	71
51	Flow visualization for a coaxial rotor system [18]	72
52	Rods for supporting gear-clamps (from first prototype)	73
53	Hub used to transmit motion of the lower motor to the rotating shaft (from first prototype).	74
54	Lower propeller adapter (from first prototype)	75
55	Upper propeller adapter(from first prototype)	76
56	Rotary shaft (from first prototype)	77
57	Lower propeller mount with rods (from first prototype).	78
58	Lower propeller mount with rods and clamps (from first prototype).	79
59	Upper propeller mount with rods (from first prototype).	79
60	A front view of the first prototype of the rotor pitch adjustment mechanism, assembled.	80
61	Metal shelf	81
62	Custom hub for attaching the twisted blades to the shaft	82
63	A labeled rendering of the final full flight vehicle	83
64	Final flight vehicle.	84
65	Final flight vehicle	85
66	Final flight vehicle	86
67	Final flight vehicle	87
68	Final flight vehicle	88
69	Central support tube	89
70	Upper shaft adapter	90
71	Wedge adapter	91
72	Adapter for using rectangular blades on wedges	92
73	Quadrotor sizing results from eCalc.	93

74	Final render of the custom vending machine	94
75	Quadrotor safety guards	95
76	Machining the lower propeller safety guards	96
77	Safety selection	97
78	Aerodynamic test in B2	98
79	Preparing for a hover test in Moore 300	99

1 Abstract

Team Peregrine has developed a unique solution to internal personal delivery within crowded, chaotic, and geometrically-challenging environments. Aerial vehicles are necessary to navigate these environments where traditional ground-based approaches fail. Challenging internal environments include sports stadiums, concert venues, and convention halls. Here, customers are disserved by waiting in lines and would benefit from personal delivery.

Our original design, the OXcopter, features two large contra-rotating propellers above a standard quadrotor configuration: a hybrid design for ease of control and efficient flight. The quadrotor simplifies vehicle control. The large propellers provide efficient lift by maximizing rotor disk area per vehicle footprint. This creates significant efficiency advancements compared to other multirotor systems which use only a fraction of their footprint for lift. In fact, the OXcopter consumes 24% less electrical power than a quadrotor of the same size and weight.

The delivery system is designed to operate autonomously. The vending machine is responsible for dispensing the payload into the vehicle's carriage. The vehicle then flies to its destination and lowers the carriage to complete the delivery.

The computation subsystem provides autonomous flight control, mapping, path planning, and obstacle avoidance. The LiDAR generates a map of the vehicle's surroundings, and navigation is guided through waypoints. Heavy computations are performed off-board to reduce the weight of the vehicle.

Team Peregrine has designed and built a novel vehicle and achieved flight. The OXcopter has a 27" diameter footprint, small enough to fit through doorways, and weighs 3kg.

2 Executive Summary



Figure 1: The OXcopter

Team Peregrine’s personal delivery solution was designed to operate in indoor environments that do not have an automated solution due to a variety of challenging constraints. Our original design, the OXcopter, is not only versatile enough to be a superior choice in disorganized settings but also offers high efficiency over other flight vehicles in lifting significant payloads. This has the potential to bring the convenience of personal delivery to customers where it has previously not been possible, a need that is well established in other capacities. Partnering with the Hershey Company, the proof of concept for our delivery system is the successful delivery of a chocolate bar to a customer.

The majority of the effort of this project was spent on the design, fabrication, and testing of the OXcopter, a hybrid design which consists of two large contra-rotating propellers above a standard quadrotor. Specifically, selecting the proper motors and propellers for both the OX (contra-rotating propellers) and the quad (standard quadrotor) systems and designing the contra-rotating assembly was crucial. The motors for the OX, as there were no off-the-shelf contra-rotating ones available at our scale, had to provide enough torque to generate the lift required for our vehicle and have a hole through the middle for our design to work. The tube that supported the upper motor and rotors had to be custom made in order to allow passage wires through the middle and carry current itself as the ground in the motor circuit. We selected two different propellers, twisted and rectangular, for the vehicle. Both fit in our maximum footprint of 66cm and could be inclined for experiments. The twisted blades performed better, but they were much more expensive than the rectangular blades.

One of the major unknowns of this project was how the lower rotor would behave in the wake of the upper rotor. The expert assumption was it would need to be inclined proportional to the flow rate of the incoming air. To test this, we designed a method to incline both the rectangular and twisted blades via 3D printed wedges of discrete angles. From these experiments, we determined that there was in fact no benefit to inclining the lower rotor (in fact, it decreased the system's performance). Our experiments showed that the vehicle was able to generate the thrust required for flight. We achieved max thrust using a pair of twisted blades with no incline of the lower rotor. Our experiments also showed that the torques of the two large rotors can be balanced at a condition where they generate enough thrust to fly.

The quadrotor subsystem was designed to fit within the footprint of the OX. Because the OX assembly was designed to provide most of the lift, the motors and propellers for the quad were chosen so that the quad could lift itself (frame, motors, and propellers) as well as steer the vehicle. This subsystem also consisted of four custom landing feet that supported the vehicle during testing.

One goal of the Peregrine Parcel delivery system was that the system would not require human interaction. In working toward this goal, the carriage and vending subsystems were designed. The carriage was mainly constrained by the type of payload, weight, and safety. A winch system lowered a lightweight basket into the vending machine, where candy was dispensed, before raising it for takeoff. The vending machine consisted of eight drawers that were able to slide out for loading and would vend the requested candy bar into the carriage for delivery by the OXcopter.

In order to achieve a fully autonomous system, a series of high-level robotic tasks had to be executed. To complete an order, the vehicle must localize itself within a map of the environment and then plan a path from its current location to the requested destination all while avoiding obstacles. The algorithms required for such a task are complex and time intensive. To increase the rate at which we could process incoming data, we opted to move the majority of the computation to a grounded base station computer. For this we confirmed that the incoming data rate could be supported by existing wireless access points on the market. By the end of the project, a localization algorithm that used information gathered by the on-board sensors to calculate the vehicle's position within its environment had been successfully implemented. This calculation was done on the base station computer, demonstrating the validity of the network's speed.

In order to allow us to safely test the vehicle in flight, we designed and built a killswitch board that could switch power to the motors. The board is designed to dissipate the power generated by up to 120 A of current, 40A more than required for the motors running on a 5S battery, and is activated and deactivated through a switch on the transmitter. To power the compute suite, namely the ODroid, Asus Xtion Pro, and the LiDAR, we designed and built a 5V regulator capable of providing up to 6A of current. The board also provides protection against current spikes from the motors.

A physical safety system adds extra protection for people who may be interacting with the OXcopter. The safety system was designed to be lightweight and strong. It consists of carbon fiber composite hoops serving as propeller guards that are supported by carbon fiber rods. This, along with the addition of a wire mesh across the guards, prevents unwanted

contact with the rotors. The lower (quad) safety system was assembled on the vehicle, but the upper was not due to time and cost constraints.

Team Peregrine has designed and built a novel vehicle and achieved flight. The OXcopter has a 27" diameter footprint, small enough to fit through doorways, and weighs 3kg. And while a fully autonomous delivery was not achieved, the subsystems that were successfully prototyped represent the necessary early iterations of making this a reality.

3 Statement of Roles and External Contributions

3.1 Anna Brill

My primary contributions were to the design and execution of the thrust stand experiments. This involved organization, propeller balancing, and experimental set up. I assisted with machining some components and with flight experiments. Additionally, I spearheaded the poster efforts. I also knit everyone hats.

3.2 Alissa Johnson

I contributed primarily in the data collection and experimentation aspects of the project. This involved recording data in an organized and orderly fashion, setting up experiments, and helping to analyze the data thereafter. I machined some structural components. My CAD efforts mostly involved creating large assemblies, including the final vehicle assembly. I was also in charge of Team Morale. Finally, I took it upon myself to take many photos, videos, and time-lapses to document our work. I was always prepared to snap a photo of a teammate caught sleeping on the foam.

3.3 William Johnson

I handled the purchase orders and finances for the team. I was involved with sizing the vehicle and selecting the components for it. I helped with data collection and analysis, design and manufacturing of many parts, and authored the final code for the carriage & vending machine demonstration at Senior Design Day.

3.4 Benjamin Kramer

I set up the ROS development environment and the LIDAR to work in it. I also configured the flight equipment and the Pixhawk to work with our custom vehicle. I did electronics component selection and designed the boards used on the OXcopter. I also helped with experimentation, and manned flights during testing.

3.5 Rachel Rusonis

My primary contributions were in the realm of mechanical design, including modeling of assemblies in CAD and designing custom components. This also included aiding in the fabrication and assembly of these parts, making modifications to subassemblies as required during testing. During experiments, I helped with data collection across many trials and configurations, modifying the test setup as needed.

3.6 Cameron Zawacki

My primary work involved the computation subsystems required for autonomous operation. This involved setting up the ROS environment on the ODROID and configuring the HectorSLAM algorithm. I put together and set up the base station computer along with putting together the network for wireless data transmission. I also had a hand in the software and electronics running in the dispensing system as well as helped with the rest of the team in collecting all of our data.

3.7 Advisors

Dr. Nick Stapp from Hershey provided project motivation and relationship with Hershey.
Dr. Paul Pounds from the University of Queensland in Australia advised us throughout the process of designing a novel flight vehicle.
Dr. Mark Yim, from the University of Pennsylvania advised on all aspects of the system.
Dr. Bruce Kothmann, from the University of Pennsylvania, provided help with analysis of experimental data.
Earn Sarkornpan, our Teaching Assistant, helped with project planning and keeping us on schedule.

3.8 Outside Sources

Solidworks was our design program of choice. We used ROS and the HectorSlam library. ModLab donated a Pixhawk to us. We also used the RC Benchmark software, Arduino and libraries for our vending machine, LoggerPro for data collection, and donated foam for flight testing to prevent damage to the vehicle.

4 Background

People desire the convenience of personal deliveries. Some deliveries occur in crowded, chaotic, and geometrically-challenging environments. These environments, hereafter referred to as “chaotic environments,” are difficult to navigate. Thus, personal delivery within chaotic environments is challenging. While humans can navigate around obstacles, their drawbacks include slow speed and high expense. Existing ground-based robotic systems fail in non-uniform spaces because their mechanical design constrains their movements such that a complete delivery path is impossible to navigate. Stairs, high grade inclines, and ground clutter are common challenges for typical wheeled robots. Examples of environments with these features include sports stadiums, concert venues, and convention halls. Here, customers are disserved by waiting in lines and would benefit from personal delivery. In fact, US sports fans said that they would be willing to spend an additional \$20 for food and beverages if wait times were cut in half [1].

An aerial delivery system would avoid the problems that both human and autonomous ground-based systems present. Our system was designed and built for internal deliveries in the Pennovation Center. The system is capable of carrying a payload of 300 g, and it has the necessary infrastructure to autonomously deliver chocolate bars to all three floors of the building.

The Pennovation Center (Figure 2) is a unique environment which combines offices, lab spaces and production areas to facilitate collaboration between researchers and entrepreneurs. Each of the three floors offer something different. The first floor is reserved as separate office spaces for partnering companies. The second floor is a co-working space, and the third floor is an open laboratory space. The collaborative environment at the Pennovation center is facilitated by modular design of work spaces and testing areas. Many areas do not serve a single purpose and are reconfigured as different people adapt them to their needs. This creates challenges for ground-based delivery systems because there may not always be a clear path for each delivery. As a result, the environment of the Pennovation Center presents many more challenges than an office with a standard cubicle configuration. Thus, the Pennovation Center is a valid location to demonstrate our internal delivery drone.

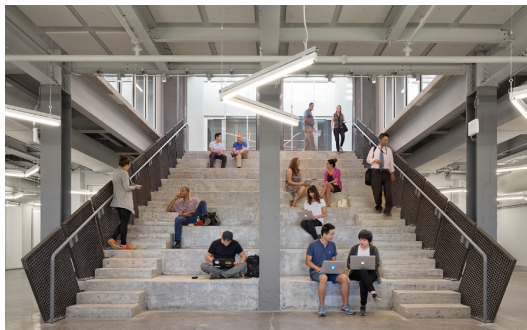


Figure 2: Staircase from the second floor coworking space to the third floor lab space in the Pennovation Center [2].

4.1 Delivery Environments

Personal internal delivery systems exist across many different fields. Hospitals are constantly transferring items such as linens, medication, food, lab test materials, or medical equipment between rooms, labs, and nursing stations. Within larger businesses, internal correspondence is delivered to different divisions and departments. Hotels make personal deliveries to their guests who request towels, sheets, toiletries, or other room services. In large stores, cash is typically transported between each cashier and a strong room multiple times a day. These situations are well-suited for human delivery and, more recently, autonomous ground-based systems. These autonomous systems are designed to speed up delivery time while allowing staff to spend less time running around making deliveries and more time doing their jobs.

However, some environments are not suitable to personal deliveries in the traditional sense. Crowded, chaotic, and geometrically-challenging environments make human and ground-based delivery systems slow or impossible. An aerial system will enable personal deliveries in environments that do not typically offer this service. Locations like sports stadiums and convention halls have separate areas for food vendors, supplemented by occasional walking vendors. In these situations, a customer must leave his or her seat to wait in line for concessions. In doing so, they may also disrupt surrounding guests. In locations with walking vendors, guests could end up waiting 20 minutes or more for the appropriate vendor to reach their section [3]. Moreover, while hotels have organized and regular layouts which make navigation straightforward for robots, other buildings have irregular and variable layouts. Deliveries within these types of buildings have not been automated because of these challenges.

In order to effectively deliver items directly to customers, delivery solutions should be well suited to the environment in which the delivery will take place. Here, two types of environments will be considered: controlled environments and chaotic environments. Controlled environments have engineered surfaces or paths to help guide navigation within the space. Chaotic environments are environments which are typically crowded or architecturally complex, rendering them difficult to navigate.

4.1.1 Controlled Environments

In controlled environments, autonomous delivery is not challenging: personal delivery is already well established and fairly efficient. Controlled environments are those that already have a clear, navigable path from Point A to Point B. These engineered paths can be easily navigated by ground-based delivery systems. Thus, in controlled environments, ground based personal delivery prevails.

Delivery Solutions for Controlled Environments

Delivery Drivers

Delivery drivers use roads to guide their navigation to the customer's requested delivery location. Delivery drivers are widespread and versatile. Many restaurants offer a food

delivery service as a convenience to their customers. Additionally, innovative food delivery solutions like Grubhub, Uber Eats, and GoPuff, have increased the convenience of personal food delivery. Delivery drivers are not yet an autonomous delivery solution; however, with the development of autonomous cars, this could soon become a reality.

Tug Robot



Figure 3: The TUG robot in a hospital [4].

The TUG is an autonomous robot (Figure 3) used for internal transportation of materials within hospitals. The system has an internal map of the hospital which it uses in combination with on-board sensors to navigate hallways and reach its destination. The robots are capable of towing 1,000 lbs, communicating with automatic doors and elevators, and running for up to 10 hours with intermittent charging [4]. Three TUGs were deployed at the University of Maryland Medical Center in 2004, and, within the first year, cycle time for drug delivery was reduced from 74 minutes to 30 minutes. These robots saved nurses 6,123 hours in drug tracking trips and improved delivery reliability by 23%. Currently, the TUG robots are being used in hospitals across the country [5].

Savioke Room Service Robot

Savioke has developed the Relay robot for delivering room service items in hotels (Figure 4). This robot is capable of carrying small items from the front desk, such as towels, drinks, and snacks, to guest rooms. Deliveries typically take less than five minutes. The robot was developed to speed up delivery time and free hotel staff from running errands so that they could focus on guest experiences. These robots have made over 52,000 autonomous deliveries across several different hotel chains [6].



Figure 4: The Relay robot being loaded for hotel delivery [7].

Mailmobile Automatic Mail Delivery

The Mailmobile (Figure 5) is an automated robot that can deliver mail from a central location to individual employees. It is capable of navigating multiple floors. The guidance system is an invisible fluorescent that is applied over existing surfaces. The robot uses ultraviolet light and photoelectric sensors to follow the paths. The system has obstacle detection, so that it will stop if there is an object in its path. The overall dimensions of this robot are 24" width, 73" length, and 52" height. The system weighs 590 lbs, travels at 100 ft/min, and has a capacity of 800 lbs on level surfaces. This system is ideal for a flat area where lines can be drawn for the robot to follow and where obstacles will not be a frequent problem [8].



Figure 5: The Mailmobile automatic delivery system [8].

Restaurant Delivery Drone

Infinium Robotics is a Singapore-based company which is developing drones to deliver food in restaurants. When integrated with restaurant work flow, kitchen staff will load food onto

these delivery drones, which will fly to a central pickup location for waiters to collect the food and deliver it to tables. To ensure the safety of restaurant customers, the drones will not fly any lower than eight and a half feet in the air so that they do not bump into anyone. This product is currently available for pre-order [9].

4.1.2 Chaotic Environments

In chaotic environments there are no simple delivery paths. People, ground clutter, and stairs inhibit the functionality of ground-based or wheeled systems by minimizing the number of possible start and end locations. A chaotic environment is therefore not the optimal environment for this type of system. Aerial vehicles are necessary to navigate chaotic environments. When constraints would have otherwise precluded the possibility of a complete delivery route for a ground based system, an aerial vehicle can navigate a more complex environment. Currently, there are no commercial solutions to personal delivery in internal chaotic environments. Team Peregrine plans to bring personal delivery to this space. (For example images of chaotic environments, see Appendix Figures 46, 47, 48, and 49,).

Delivery Solutions for Chaotic Environments

Free Motion Handling

The German Robotics Firm Festo has created a bubble drone that can pick up objects and autonomously navigate through its indoor surroundings (Figure 6). The drone consists of a 54" diameter helium-filled balloon and eight propellers for control and navigation. The gripping system uses a helium balloon arm to absorb delivery items into the body and release the payload upon arrival at its destination. Festo hasn't discussed commercialization of this product yet, but they envision that it will be used to help increase productivity in production lines [10].



Figure 6: Festo's drone delivering a small item [10].

Amazon Delivery Drone

Amazon is working to develop Prime Air, an aerial delivery system designed to deliver small packages to local customers in 30 minutes or less (Figure 7). They will be able to service customers within a 15 mile radius of a Prime Air delivery center [11]. They are developing



Figure 7: Amazon Air drone [11].

a fleet of hybrid flight vehicles capable of vertical take off and landing, designed to fly at an altitude of 400 ft [11] [12]. Prime Air demonstrated its first successful public, United States drone delivery on March 24, 2017 when a quadrotor delivered a box of sunscreen to a MARS 2017 conference in Palm Springs California [13]. Amazon's drones are capable of making deliveries without the use of pre-existing paths. Further, these vehicles are designed for outdoor flight at high speeds and would not be suitable for indoor environments.

5 Objectives

The primary objective of Team Peregrine is to design and build an internal delivery drone that can autonomously deliver chocolate bars within the Penovation Center. The delivery drone will be optimized to minimize propeller wash and noise for a payload of 300 grams. In order to fully automate the overall delivery system, several subsystems will be necessary. For instance, the integration of a dispensing subsystem will eliminate the need for humans to load deliveries onto the vehicle. A package-lowering system will allow items to reach customers with minimal effort on the part of the customer. The fall semester deliverable will focus primarily on the drone itself and the preparation of any computational systems or electronics necessary for stable flight. Spring deliverables will focus on the integration of all subsystems, solving the path-planning and navigation problems, and implementing a safety system.

The project consists of three different subsystems: the aerial vehicle itself, the payload dispensing and delivery, and the computational system. Quantified descriptions of basic, intermediate, and reach goals for each component are summarized in Tables 1-3 below.

5.1 Flight Vehicle

Table 1 delineates three different stages of vehicle deliverables. All stages require the minimization of sound produced by the rotors. Since the delivery vehicle is meant to increase convenience for customers, there should be minimal distractions from or interferences with customers' tasks. Consequently, at a distance of half a meter from the copter, the resulting

Table 1: Vehicle Deliverables

Goal Type	Description	Quantification
Reach	A designed and built aircraft capable of controllable flight with the required physical payload of chocolate	300g payload
	Flight time with carriage system integrated	10 min flight time
	Sound is minimal	<70 dB of noise 0.5m away from copter
	Active and Passive Safety System	Path planning to minimize flying over people
Intermediate	A designed and built aircraft capable of controllable flight with an artificial payload	300 g payload
	Flight time	10 min flight time
	Sound is minimal	<75 dB noise 0.5m away from copter
	Passive Safety System with plans for active	Propeller guards, landing feet, foam padding
Basic	A designed and built aircraft capable of stable hovering with an artificial payload	300 g payload
	Flight time	10 min hover time
	Able to measure sound produced by copter	<80 dB noise 0.5m away from copter
	Passive Safety System	Propeller guards, landing feet, foam padding

noise would preferably be no louder than the average conversation, which is typically 60 dB [14]. Further, in order to achieve the reach goal of complete autonomous delivery by spring, an important first step is hovering with an artificial payload of 300g for the desired flight time. Hovering, however, does not introduce all of the control complications that come with full flight. Further, an artificial payload can be affixed to the copter which eliminates some imbalances that may be introduced by a tethered physical payload, which can shift during flight.

5.2 Dispensing and Delivery

Table 2: Vending and Carriage Deliverables

Goal Type	Description	Quantification
Reach	Carriage package carrying system is integrated with the drone	18 cm diameter footprint, <50g
	Package can be delivered at a distance	Successful delivery
	Full vending machine, integrate with carriage and vehicle	dispense candy, vehicle landing pad
Intermediate	Carriage system is designed and built, not yet integrated	18 cm diameter footprint, <100g
	Proof of concept vending machine, integrated with carriage	can dispense candy & accommodate carriage
Basic	Carriage system is designed to be integrated with the vehicle, but not built or integrated	18 cm diameter footprint
	Custom vending machine designed to integrate with carriage	CAD, Bill of Materials, Engineering Drawings

Table 2 describes the dispensing and delivery goals which allow for a fully automated delivery system. A custom vending machine will be responsible for autonomously dispensing the requested payload directly into the vehicle’s carriage. The carriage will be designed to carry up to 300 grams of chocolate and fit into a 7” diameter footprint, as constrained by the dimensions of the rotor layout. The container will be lowered via a winch system to allow deliveries from a distance.

5.3 Computation and Sensory Systems

Table 3: Computation and Sensory Deliverables

Goal Type	Description	Quantification
Reach	Flight controller integration with sensor input	Achieve stable flight with sensor array on board
	Sensor data relayed back to base station	Maintain two way communication between craft and base station
	Craft can localize itself within a map of the building	Runs SLAM
Intermediate	Flight controller integration with sensor input	Achieve stable flight with sensor array on board
	Sensor data relayed back to base station	Maintain two way communication between craft and base station
Basic	Basic flight controller integration with sensor input	Achieve stable flight with sensor array on board

Table 3 delineates three different stages of computation and sensory deliverables. The first stage is integrating a basic flight controller. This will allow the OXcopter to maintain stable flight off the ground while holding the array of sensors necessary to operate autonomously. The intermediate and reach goals are the development of the autonomous computations. This would include communication with the off-board base station where the LiDAR and RGBD sensor data will be used to localize the OXcopter within a map of the building.

5.4 Final Deliverables

In addition to the quantified metrics for the subsystems outlined above, the reach goal for this project was to integrate all systems and achieve a complete, autonomous delivery with no human interaction. In order to demonstrate that the Peregrine Parcel delivery system is capable of delivery in an indoor chaotic environment, the final reach demonstration would consist of an automated candy dispenser and a drone capable of navigating through the Pennovation Center, delivering chocolate to a specified location, and returning to the docking station.

6 Design and Realization

6.1 Summary of Design Considerations

Before deciding to make a unique flight vehicle, the merits of existing solutions were evaluated with respect to the metrics that our problem statement defined. The standard quadrotor offered advantages in off-the-shelf compatibility. This system would likely only require tuning of the controls before flight could be achieved. However, this solution did not lend itself to modifications that would allow for less propeller wash, reduced noise, and increased efficiency. Therefore, other existing solutions were considered. Dr. Paul Pounds developed the Y4 quadrotor that combined three lower propellers with a large propeller above. In his research, he found that this design offered greater efficiency, but the single large propeller introduced an unbalanced torque on the system, which made control quite challenging. Based on this analysis, the OXcopter was conceptualized. It combines a lower quadrotor with upper contra-rotating propellers to balance torques.

6.2 Vehicle Selection

The design space for this project is personal delivery within internal chaotic environments. As mentioned, delivery within chaotic environments requires a flight vehicle to navigate above the obstacles in the space. Several vehicle configurations were considered and a summary of the evaluations of various system level solutions is presented in Table 4 below. Further description of each solution follows.

Table 4: Comparison of System Level Solutions

Solution	Advantages	Disadvantages
Hybrid Multicopter Airship	Minimal noise & wash	Significant volume necessary to offset load to buoyancy
Triangular Quadrotor (Y4)	High efficiency	Field of study is very new Increased mechanical & control complexity
Standard Quadrotor	Mechanically simple Straightforward control Maneuverability	Large power consumption Less lift capabilities Decreased flight time
OXcopter	Decreased electrical power consumption Ease of control Increased thrust-to-weight ratio	Large vertical spacing is optimal More expensive

6.2.1 Hybrid Multirotor Airship

System Description

Drones in populated environments, especially indoors, can be noisy and thus disruptive to passerby. A delivery system where buoyancy is used to offset the weight of the vehicle and payload would not require rotor thrust to generate lift. This hybrid system would only use rotors to control directionality, which would be less noisy than the larger rotors needed to lift the entire weight of the craft. Propeller wash from the rotors will also be minimal in this situation.

System Evaluation

A combination of rotors and a lighter-than-air balloon was considered as an option to reduce required rotor power and therefore noise. Since size is a main constraint on our flight vehicle, the amount of space required per amount of lift was considered. For a system that generates lift via rotors, such as a quadrotor, increasing the length of a 1" height propeller by 1" results in a corresponding increase in revolved volume of 28%. This increase in volume with a Tiger F60 motor, according to the specifications for 50% throttle on 5" and 6" propellers, will lift an additional 100 grams at 50% thrust [15]. The equivalent volume increase for an ideal helium balloon given by:

$$F_{net} = (\rho_f - \rho_h)gV - mg \quad (1)$$

will only lift an additional 0.38 grams.

Even an ideal helium balloon would not generate enough lift to rationalize offsetting some of the load to buoyancy in confined environments.

6.2.2 Multirotor Systems

Multirotor systems are advantageous due to their mechanical simplicity, maneuverability, and ease of control. Disadvantages of multirotor systems include decreased effective rotor area per vehicle footprint (compared to helicopters, which utilize the entire footprint), leading to greater mechanical power consumption, decreased lift capabilities, and shorter flight times. Despite these disadvantages, multirotor systems are a good option for many applications, including navigating tight spaces. While there are various multirotor configurations which have their own advantages and disadvantages, we can narrow the field with some general insights.

The simplest and most popular multirotor configuration is the standard quadrotor. Multirotors with fewer than four rotors add unnecessary mechanical complexity to the system and, in some cases, asymmetry to the control scheme. Aerial vehicles with more than four rotors, such as hexacopters and octocopters, have become quite popular with aerial photographers and hobbyists due to their greater stability. However, increasing the number of rotors in this fashion further decreases the effective rotor area per vehicle footprint (See Figure 8), severely limiting payload capacity given the strict size constraints of indoor flight.

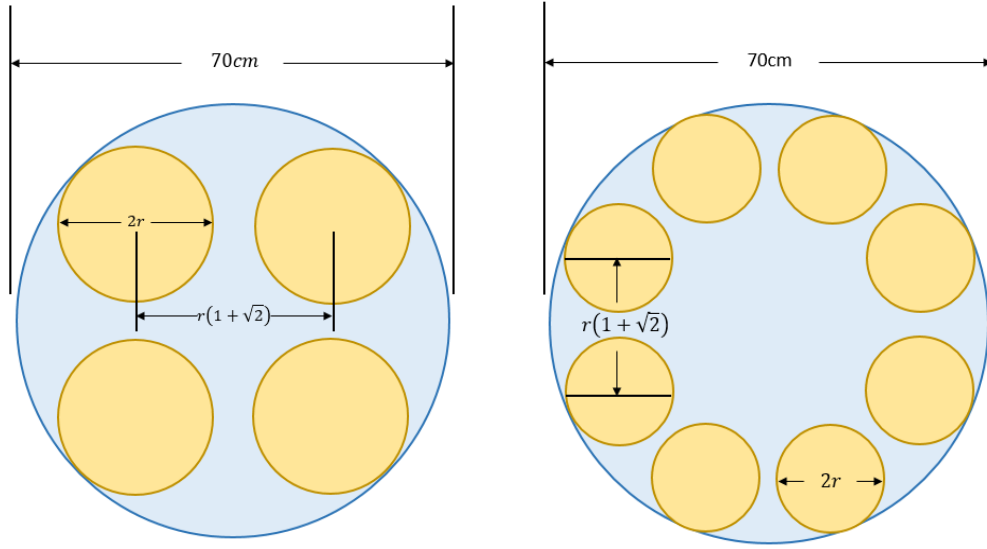


Figure 8: Multirotor effective rotor area for (a) standard quadrotor and (b) standard octotor. Working through the geometry gives (a) $r = 12.9\text{cm}$; Area Fraction = 54.6% and (b) $r = 8.4\text{cm}$; Area Fraction = 46.4%.

6.2.3 Y4 Triangular Quadrotor

System Description

The Y4, or “triangular quadrotor” was developed as a more efficient quadrotor configuration. As seen in Figure 9. It has a large central rotor that is responsible for all of the vehicle’s thrust while three smaller boom rotors both control the vehicle and counter the drag torque of the large central rotor [16]. By maximizing the effective rotor area per vehicle footprint, the Y4 combines the efficiency of a helicopter with the maneuverability of traditional multirotor vehicles.

System Evaluation

When compared with an identically-sized standard quadrotor, the Y4 has demonstrated a 15 percent power improvement [16]. The theoretical limit of this gain is as high as 25 percent, but further verification is required. The Y4 trades this increase in efficiency with increases in complexity. For example, the Y4 experiences a natural precession effect due to a large gyroscopic moment about the large rotor. This problem is solved with a flapping hinge at the base of the main rotor, allowing it to instantly achieve dynamic equilibrium, but adding mechanical complexity to the system. The control of the Y4 is similar to that of a standard quadrotor, with a few more complexities. Moreover, this control system has not been as extensively studied as that of the standard configuration. The Y4 would be an attractive alternative in the event that the standard configuration can’t meet the project’s objectives.

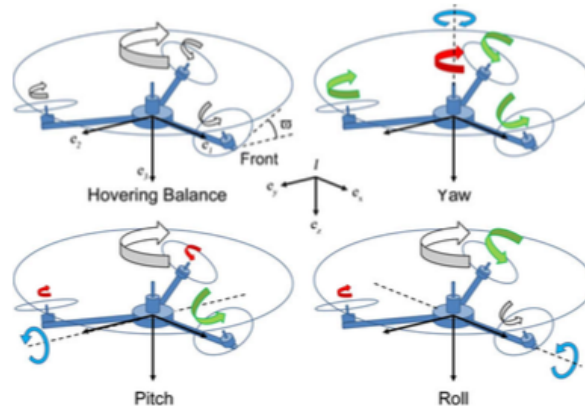


Figure 9: Triangular quadrotor maneuvering controls. Arrow sizes indicate relative rotor velocities (white arrows are constant) [16].

6.2.4 Standard Quadrotor Configuration

System Description

The standard quadrotor configuration utilizes four coplanar rotors to control the aircraft. Variations in thrust between the rotors allow the craft to roll, pitch, and yaw without the mechanically complicated swashplate used on helicopters. This mechanical simplicity means quadrotors require much less maintenance. This, along with their simple control scheme, makes quadrotors an attractive choice for many applications. Also, the standard model is widely used and has a large research base. Controllers for the standard design have been through extensive testing and are thus robust and streamlined.

System Evaluation

The main disadvantage of the standard quadrotor configuration is the high disk loading as a result of its low effective rotor area per vehicle footprint. This makes quadrotors a less-attractive choice for applications that involve carrying payloads for long flight times where the vehicle size is strictly constrained (the disk loading could be reduced if the vehicle were made larger). Additionally, for our application, this higher disk loading would lead to greater noise and propeller wash. We now consider a system that aims to combine the simplicity and maneuverability of the standard quadrotor configuration with greater carrying capacities, flight times, and added safety benefits.

6.2.5 Contra-Rotating Rotor Configuration

System Description

Drones intended for indoor flight or cramped spaces have their size constrained by the width of doorways, hallways, and other obstacles. This limits their capacity to carry large payloads due to the increased power requirements of smaller rotor disk areas. Additional rotors increase the available lifting surface area, but usually cannot be accommodated due to these size constraints. To work around this, a system where rotors are stacked vertically

can provide the effective rotor surface area needed to achieve the desired lift without such prohibitive power consumption [17].

System Evaluation

Coaxial rotor systems will consume less electrical power than a single rotor carrying the same weight. The ideal electrical power required to drive a single rotor is derived from the thrust equation, assuming a zero surrounding air velocity. When surrounding air velocity is non-zero, actual electrical power consumption deviates from the ideal. This occurs where the lower rotor is affected by the downwash of the upper rotor. That is, the fast moving air exiting the upper rotor affects the performance of the lower rotor, similar to a helicopter in climb. The effective power factor describes this deviation of actual electrical power consumption from the ideal.

$$\sum P_{\text{coaxial}} = \kappa_{\text{eff}} \sum P_{\text{ideal}} \quad (2)$$

Professor Paul Pounds of the University of Queensland demonstrated the benefits of coaxial rotors with his Stackrotor system [17]. The Stackrotor is an aircraft comprised of one or several rotor modules, each with a pair of contra-rotating propellers. There is significant vertical spacing between these propellers to minimize the effect of the wake velocity of the higher propeller on the performance of the lower propeller. Pounds was able to show energetic benefits from stacking more rotor modules as long as each additional module did not add a significant amount of mass to the aircraft. The power advantages of stacked rotors could be leveraged while maintaining the simplicity and control advantages of a standard quadrotor by stacking two large, contra-rotating rotors above a small quadrotor. The contra-rotating assembly will provide most of the thrust of the vehicle. Because the propellers will be rotating in opposite directions, their torques will be balanced, eliminating the unbounded yaw precession of the Y4 design. The small quadrotor would be used to maneuver, and will not provide much additional lift.

The OXcopter configuration will have a similar control scheme to that of a quadrotor. The coaxial rotors will be throttled up or down at a specific speed ratio maintain balanced torques and to change height. The small quadrotor will use an off-the-shelf controller for yaw, pitch, and roll control.

While this coaxial configuration enables a vehicle limited by rotor diameter to achieve greater thrusts via multiple stacked rotors, it comes at the cost of significant vertical spacing. An ideal stacked configuration would have enough vertical space between rotors such that the wake energy of above rotors is absorbed by viscous air forces allowing rotors to behave as if in isolation. Pound's Stackrotor with only two modules (4 rotors) approached the height of a person (1.8m). The Stackrotor used rotors with a 70cm diameter. The rotors used for the Peregrine Parcel's OXcopter will be 66cm, so the required vertical spacing for maximum energetic benefit might be similar. This is impractical for a delivery drone which should be maneuverable. Yet, efficiency advantages are still possible with smaller rotor spacing. In this case, the rotors will not behave as if in isolation, but the lower rotor will operate in what is known as the vena contracta (contracted wake) of the upper rotor. Then, the downwash of air from the upper rotor will only affect half of the disk area of the lower rotor [18]. For the OXcopter, the necessary rotor spacing to achieve this will be 6.5 inches.

Configuration Selection: The OXcopter

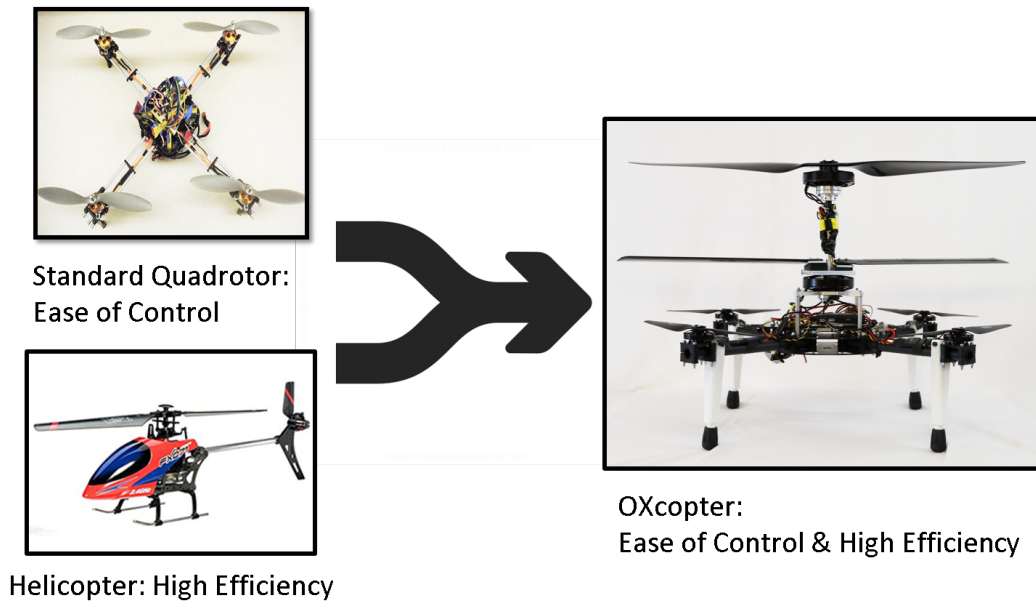


Figure 10: Motivation for the OXcopter [19][16].

To maximize the efficacy of our delivery system, we require an efficient flight vehicle. Specifically, for indoor delivery applications, the flight vehicle should be minimally disruptive to the surrounding environment. In general, a more efficient flight vehicle will be less disruptive. That is, the downwash of fast moving air that exits the propellers could be an annoyance indoors. The speed at which this air moves is correlated to the power consumption of the vehicle. Thus, a more efficient vehicle will have less downwash. Additionally, efficient vehicles are quieter because the noise is correlated to the speed at which the propellers spin. Larger propellers can generate the same thrust as smaller ones while spinning at slower speeds.

The selected flight vehicle configuration for our delivery system will be the first ever OXcopter, a unique multirotor configuration consisting of two large contra-rotating propellers above a standard quadrotor. This design was selected primarily for its efficiency advantages over other multirotor systems which use only a fraction of their footprint for lift.

The design for the OXcopter was motivated by two existing aerial vehicles. Quadrotors can be easily controlled with many off-the-shelf controllers, but suffer from lower efficiencies for their footprints. Helicopters are much more efficient because the large central rotor takes up most of the vehicle's footprint, but, to counter its drag torque, resources must be diverted to a tail rotor. Our hybrid vehicle design combines the simplicity of the quadrotor with the greater efficiencies of a helicopter, as demonstrated in Figure 10.

6.3 Contra-Rotating Propeller Subsystem

The contra-rotating sub assembly, which we call the OX, maximizes the rotor disk area to increase efficiency. The rotors spinning opposite directions allows for their drag torques to balance so that the vehicle does not spin during flight, and the coaxial rotors give us more thrust for the same vehicle footprint.

The general size of the vehicle was the primary design decision. This influenced many other design considerations down the road. Considering indoor flight, the delivery vehicle would be constrained by the width of doorways. As a result, the vehicle footprint, and thus the diameter of the large central propellers should be as large as possible while still retaining the ability to maneuver through doorways. Given the American Disability Act Doorway standards, doorways are required to be at least 32 inches wide [20] (See Appendix Figure 50 for more details). Thus, an initial vehicle footprint was estimated to be 66 cm or about 26 inches in diameter. Further, for initial sizing calculations, the total vehicle weight was estimated to be 3 kg. This was determined by summing the total weight of electronic components needed for autonomous flight, estimating the weight of structural components, and accounting for 300 grams of payload weight.

6.3.1 OX Design Motivation

The motivation for the initial design of the contra-rotating subsystem stemmed from an existing product, contra-rotating motors. A contra-rotating motor, pictured in Figure 11, is a compact combination of two motors and shafts with the capability to spin the shafts in opposite directions. This was exactly what was needed to realize the OXcopter design: a simple way to spin two propellers in opposite directions. Initially, the prospect of purchasing contra-rotating motors off-the-shelf was explored. However, after primary sizing and analysis, it was determined that existing products did not offer the scale that was needed to power a large vehicle. Specifically, the commercially available contra-rotating motors which would be able to meet the propeller size specifications (approximately 26 inches) would weigh 30 lbs, or about 13.5 kg [21]. Using these motors would have caused an extremely disproportionate amount of the total vehicle weight to be the motors themselves, so this design was not selected. Even though these motors could not be used directly, the idea of a contra-rotating motor which uses a spinning shaft to spin propellers heavily influenced the design of the first prototype.

6.3.2 First OX Prototype

As Figure 11 depicts, one way to achieve contra-rotating propellers is to stack two motors directly on top of each other. In this case, the bottom motor attaches to a shaft which spins the upper propeller. The upper motor directly spins the lower propeller and has a hole to allow the shaft to pass through. This design idea influenced the initial design of the contra-rotating sub-assembly. Since commercially available contra-rotating motors would be weight prohibitive in our application, the first prototype design sought to replicate the basic structure of these motors by stacking lighter motors to create a contra-rotating assembly.



Figure 11: A commercially available contra-rotating motor for smaller flight vehicles [21].

In order to do this, it was necessary to use motors with hollow centers so that a spinning shaft could pass through. Therefore, brushless DC motors with hollow centers that would be compatible with 66 cm diameter propellers were researched. The resulting motor selection ultimately influenced many later design decisions, as described in the 'Component Design Selection' section below.

OX Component Design Selections

Motor Assembly Selection

Motor selection for the custom contra-rotating assembly was initially narrowed to brushless DC motors because these motors are typically used for multirotor UAVs. Further, requiring motors with central holes limited the brushless motor selection to the T-Motor U-Power Series Motors. Individual motor specifications were consulted to inform the motor selection decision [22] [23] [24]. A summary of the basic considerations for motor selection is presented in Table 5. First, it was important that the selected motors be compatible with the estimated 66 cm propeller diameter. Fortunately, all of the U8 Power Series motors are capable of mounting propellers of this size [22] [23] [24]. Next, as is necessary with aerial vehicles, structural components should be as light as possible. Thus, the overall weight of the motors was a major factor in the motor selection decision. The ideal motor would be the lightest motor that could yield enough thrust to lift approximately half of the 3 kg vehicle off the ground. For preliminary sizing, it was assumed that the OX would generate most of the thrust for the entire vehicle.

Another factor in the motor selection decision was the necessary input power to achieve a given thrust. The motor specification tables for the U-Power Series suggested using a 6 - 12S battery. These batteries can be very large and heavy. A lighter battery was desired for

weight minimization. Since the U-Power Motors are quite powerful, the possibility of using a smaller battery while still obtaining enough thrust was explored. In order to do this, the motor specifications were compared for various U-Power Series motors paired with 26x8.5 propellers and 22.2 V, 6S batteries. First, the U12 series motors were eliminated because they were weight prohibitive [24]. For the remaining motors, we compared the minimum throttle setting (under the specified conditions of 26x8.5 propellers and a 6S battery) which would yield approximately 1.5 kg of thrust (half the vehicle weight), as shown in Table 5. It was assumed that full throttle for a 4S battery would correspond to 65% throttle for a 6S battery, as shown in the equations below.

$$6SVoltage = 22.2V \quad (3)$$

$$4SVoltage = 14.8V \quad (4)$$

$$22.2V * \frac{2}{3} \approx 14.8V \quad (5)$$

Then, a motor which could provide approximately 1.5 kg of thrust with a 6S battery at 65% throttle would still be able to get the vehicle off the ground with a 4S battery at full throttle.

Table 5 demonstrates that the 170 Kv U8 is the best option. The U10 motors do not offer significant advantages for their added weight. On the other hand, the 170 Kv U8 is capable of generating enough thrust to get the vehicle off the ground at half throttle (assuming that the quadrotor beneath will contribute minimally to the overall thrust). This not only demonstrates that a smaller, 14.8V 4S battery is possible, but also that there is some built-in safety allowance when using this smaller battery. That is, 50% throttle for the 6S battery corresponds to approximately 80% throttle for a 4S. Then, if the weight of the vehicle was heavier than the initially estimated 3 kg, there is yet more battery power available. One drawback of the 170 Kv U8 motors is that they will require a larger power draw than the others. This was taken into consideration when selecting the battery in order to ensure that there would be enough energy available for 10 minutes of flight time.

Table 5: OX Motor Selection

Motor Type	Weight (g)	Throttle for $\tilde{1.5}$ kg Thrust (%)	Thrust at Given Throttle (g)	Power at Given Throttle (W)
<i>U8 (100 Kv)</i>	240	75	1400	84.36
<i>U8 (135 Kv)</i>	239	65	1530	93.24
<i>U8 (170 Kv)</i>	239	50	1420	97.68
<i>U10 (80 Kv)</i>	400	85	1735	112.8
<i>U10 (100 Kv)</i>	400	85	1420	95.46

OX Shaft Selection

The 170 kV U8 motors were selected to make up the contra-rotating sub-assembly. Next, it was necessary to select a central shaft which would be used, like in the design motivation, for the lower motor to transmit power to an upper propeller through a spinning shaft. The

hole in the U8 motor was 3/16", so a 3/16" diameter steel shaft was initially selected. The shaft was purchased; however, secondary operations such as adding flats to interface with set-screws were done on a Manual Mill. This shaft was 12 inches long; 2.75 inches of the shaft passed directly through the motors, 6.25 inches were used to achieve the optimal spacing between the upper and lower propellers, and the remainder extended beyond the upper propellers. That is, since the down wash of air from the upper rotor will affect the performance of the lower rotor, the rotors should be spaced far enough apart such that the flow from the upper rotor can be considered contracted by the time that it reaches the lower rotor. Then, only half of the area of the lower rotor is affected by the upper rotor's down wash [18] See the flow visualization figure in Appendix Figure 51 for more details.

Battery Selection

Even though the battery powers the entire vehicle and additional electronics, the U8 Motor Selection was the primary influence on battery sizing since these motors would be the largest current draw from the system. When selecting motors, it was already discovered that it would be possible to use a 4S battery, so battery selection was limited to 4S LiPo batteries. Next, it was important to ensure that the overall energy content in the battery would be enough that our system could fly for 10 minutes, enough time to make a delivery and return trip in the Pennovation Center. Finally, it was necessary to consider the overall weight of the battery when making a selection. The price of the battery was also considered, but this was not as important as having enough energy or being light weight. A comparison of several battery options is presented in Table 6.

A preliminary calculation for the required energy content could help narrow the necessary mAhs (milliamper hour) when sizing the battery. 4S LiPo Batteries are typically 14.8V. From the T-Motor U8 Specifications, the 170 Kv U8 should draw 97.68 W at 50% throttle (for 6S battery), which should be enough to lift the entire vehicle [22]. As a safety factor, the battery sizing was done assuming that 65% throttle was needed to lift the vehicle, that is, full throttle on a 4S battery. In this case, a single U8 would draw 175.38 W. Since the coaxial system required two U8s, twice that current draw would be needed simply for the OX. The other components such as the quadrotor motors and other electrical components will also draw current. The total power consumption was initially estimated to be about three and a half times that required for a single U8. This lead to a battery energy capacity estimate of about 368 kJ, or about 7000 mAh for a 14.8V as shown in the calculation below.

$$Voltage = 14.8V \quad (6)$$

$$FlightTime = 10min = 600s \quad (7)$$

$$PowerReq = 3.5 * 175.38W = 613.83W \quad (8)$$

$$EnergyReq = 526.14W * 600s = 368.298kJ \quad (9)$$

$$minmAh = \frac{EnergyReq * 1000(mA/A)}{Voltage * 3600(s/hr)} = \frac{368298J * 1000}{14.8V * 3600} = 6912.5mAh \quad (10)$$

Looking more closely at batteries that met this minimum energy capacity requirement, additional weight and price specifications were compared in order to make the final selection,

as can be seen in Table 6. Table 6 demonstrates that the 10,000 mAh MultiStar High Capacity Battery is the best available option. Though the Zappy Flightmax meets the minimum capacity requirements, the 10000 mAh Multistar High Capacity offers a significant capacity increase without significant cost or weight increase. The other two batteries are weight prohibitive. Thus, the 10000 mAh Multistar High Capacity Battery was selected for this application.

Table 6: Battery Comparison Summary

Name	Capacity (mAh)	Weight (g)	Price (\$)
Zippy Flightmax [25]	8,000	845	63.82
MultiStar High Capacity [26]	10,000	1035	73.38
Turnigy Graphene Professional [27]	10,000	1310	78.85
MultiStar High Capacity [28]	16,000	1400	79.64

OX Propeller Selection

As mentioned, initial propeller sizing was based on the doorway width constraint [20]. Further, after having selected the T-Motor U8 motors, their specification chart suggested using the compatible 26x8.5 Carbon Fiber blades [22] [29]. These propellers would cost \$235.90 per pair [29]. Since the OXcopter is a new design, we anticipated breaking many blades during initial flight and control test crashes. As a result, it was not desirable to risk spending a disproportional amount of the budget on expensive blades while there were many other expensive components to purchase. Twisted blades, though more efficient, tend to be quite expensive. Instead, flat rectangular blades of a comparable size were selected to be used for the contra-rotating subsystem. Specifically, 325mm Carbon Fiber Rotor Set was selected, as this would yield a tip to tip distance of approximately 25.5 inches and these blades cost only \$24.99 per pair [30].

Propeller Clamp Design

For mechanical simplicity and efficiency, multirotor UAVs traditionally use fixed-pitch twisted propellers. The coaxial rotor system (The OX) part of the OXcopter is similar to a coaxial helicopter. Helicopters have rotor heads and swash plates, similar to the one shown in Figure 12 which allow the propellers to change pitch during flight. In order to maintain mechanical simplicity in our hybrid vehicle, it was elected to fix the pitch of our propellers during flight. In order to do this, the optimal propeller pitch needed to be determined.

In order to optimize the power consumption of the contra-rotating system, a bevel gear-propeller clamp system, called gear-clamps, was designed so that the pitch of the rotor blades could be adjusted in a controlled and measurable fashion. This would accommodate experimentally finding the angle of each blade that would result in the best performance, despite the lower blade operating in the down wash of the upper blade. Helicopters use a mechanism called a swash plate to adjust the pitch of their blades, pictured as part of the rotor head in Figure 12. This idea of clamping on to the propellers and adjusting the pitch of the clamp inspired the design of the bevel gear propeller clamps. Figure 13 shows the custom designed and 3D printed parts that combine a bevel gear and propeller clamp. This system allows for the pitch of both blades to be adjusted equally in opposite directions simply by



Figure 12: A commercially available rotor head for an RC helicopter [31].

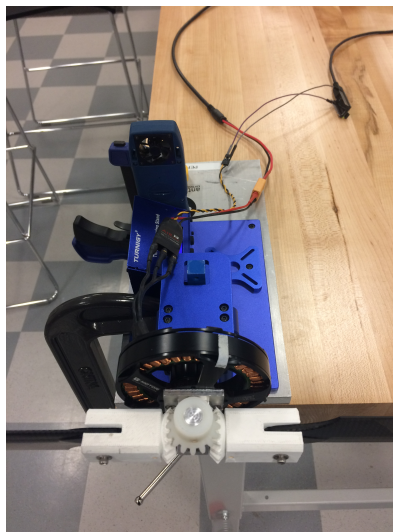


Figure 13: The bevel gear propeller clamp system during thrust testing.

turning the central bevel gear. Further, conical set screws interfaced with a circular groove in the support rod to lock the gears in place and allow for the pitch of the blades to remain fixed during tests.

OX Additional Structural Components

Additional structural components were necessary to support the gear-clamps and attach them to the appropriate motor or shaft. First, the clamps themselves were supported by rods through their center. Reference Figure 14 (a) for a visual of the design. These rods had a circular groove around their cylindrical face so as to interface with the set screw in the gear-clamp regardless of the clamp's position relative to the rod. The other end of the rod was externally threaded so that it could screw in to an adapting part, either the Lower Prop Adapter or the Upper Prop Adapter, described below. The rods were manufactured in the Machine Shop on the lathe.

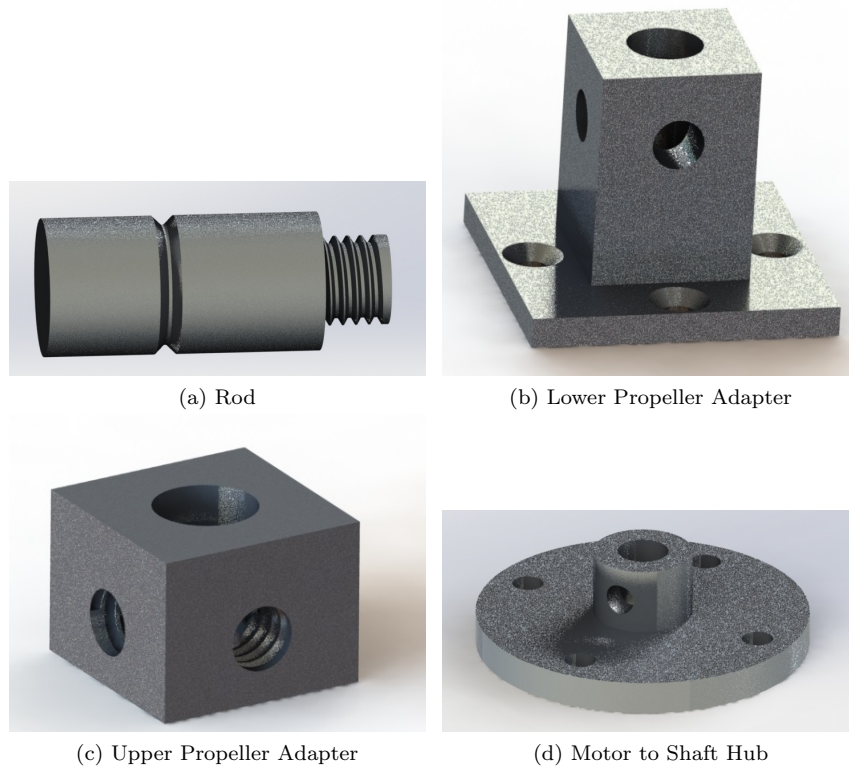


Figure 14: Renderings of structural components designed and machined in the first prototype of the OX subassembly.

The Lower and Upper Propeller Adapters had threaded holes to interface with the rods. Additionally, the lower propeller adapter had the appropriate hole pattern to interface with the rotor of the U8 motor, as shown in Figure 14 (b). This way, the lower propeller would spin with the upper motor. The upper propeller adapter, in addition to interfacing with the

rods, had a set screw to interface with the flat on the central shaft, as shown in Figure 14 (c). Then, the rotary motion of the shaft would translate to spin the upper propeller. Both propeller adapters were manufactured on ProtoTRAK mills.

Finally, in order to ensure that the lower motor could spin the shaft, a hub was designed and manufactured, as depicted in Figure 14 (d). This hub included the hole pattern of the U8 rotor as well as a set screw to interface with the flat on the shaft. The aluminum hub was manufactured on the Lathe.

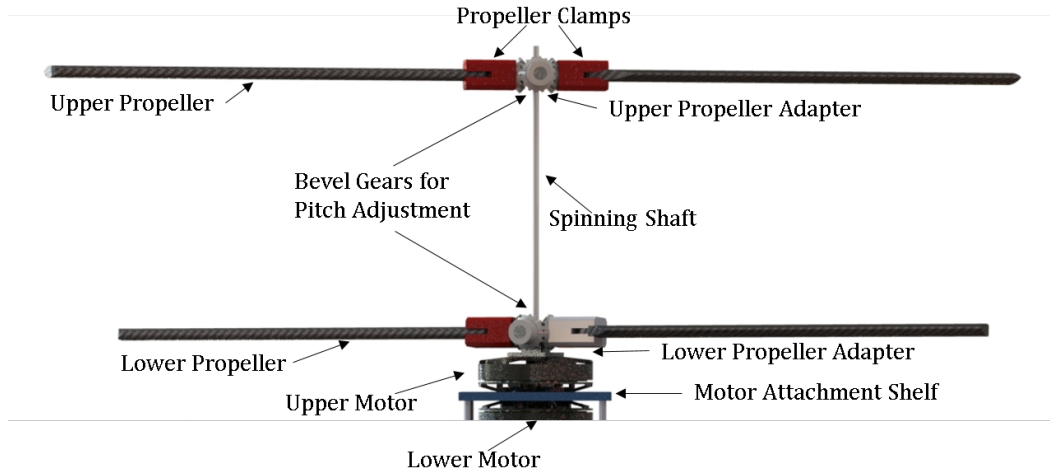


Figure 15: A rendering of the first prototype of the OX subsystem, with labeled components.

A labeled rendering of the many components which make up the first prototype of the OX sub-assembly can be seen in Figure 15. Please reference the Appendix Figures 52 - 56 for engineering drawings of the bevel gear clamp and the other components in this assembly. Additional renderings and photos of these components can be seen in the Appendix Figures 57 - 60.

OX Fabrication and Assembly

The motor assembly was attached to the flight vehicle via a shelf. The existing holes on the motors were used to attach both the top and bottom motor to the shelf. The initial prototype, made of 1/4 inch ABS, was laser cut. This part was later replaced by an aluminum shelf that was machined to a custom geometry with the ProtoTRAK (See the Appendix Figure 61). The lower prop adapter was attached to the upper motor, the rods were screwed in, and gear clamps were fixed to the rods with set screws. The shaft was then passed through the motor assembly and attached to the lower motor via a hub and set screw. The twisted blades included a mounting hub assembly, but in order to attach this to the shaft, a custom hub with set screw was fabricated (see Appendix Figure 62 for drawings and renders). Figure 16 shows this configuration fully assembled.

During thrust testing, the OX assembly was mounted horizontally to the thrust stand (explained in more detail during validation), and the free end of the rod was supported by a block with a bearing inside. However, when we did initial flight tests with the OX assem-



Figure 16: The initial design of the contra-rotating system, with a rotating shaft.

bly vertically oriented, it became clear that a spinning shaft with such a small diameter (constrained by the motor holes) would not be sufficient. Specifically, the shaft was not strong enough to withstand centrifugal forces at high speeds. That is, eccentric loading as a result of non-uniform mass distribution about the central axis resulted in an offset between the axis of rotation and the center of mass of the rotor. This is an amplifying effect where the offset would create an outward force which would induce more offset. This effect was witnessed first hand during one of the early flight tests where the shaft bent causing catastrophic failure (see Figure 17). A stronger rod would be able to withstand minimal perturbations, but it would need to be much thicker. In addition to adding weight, a thicker shaft was simply not possible given the size constraint of the central holes in the motors. As a result, the OX subassembly was redesigned to avoid a spinning shaft.

6.3.3 OX Final Design

Design Overview

The goal of the new design was to eliminate the rotating shaft. This was achieved by



Figure 17: Bending failure of the first prototype.

mounting one motor on top of a hollow rod, feeding the motor wires through a hole just above the lower motor, through both motors, and out the bottom where they could then be connected to the circuitry on the vehicle frame (See Figure 18). The lower motor was simply fixed to the stronger, aluminum shelf (See Appendix Figure 61 for drawing). This design allowed for two coaxial motors to be mounted on opposite ends of a support tube without the wires from the upper motor getting caught in the propellers mounted to the lower motor. Additionally, since the motors were spaced apart by the tube, each motor could directly spin the appropriate propeller and the support tube would remain stationary. More images of the final flight vehicle can be seen in Appendix Figures 63 - 68.

Support Tube

By eliminating the contra-rotating design, the tube would no longer have to resist centrifugal forces. Now a structural component, the tube was fabricated out of aluminum rather than steel because it is less dense. Ultimately, the size of the support tube was still limited by the finite size of the holes in the lower motor. A $3/8$ " outer diameter tube with a 0.145 " diameter central hole was selected. This way, the tube could be turned down on the bottom end to a $1/4$ " diameter, to accommodate the narrower hole diameter in the motor without eliminating the wall thickness all together. See Appendix Figure 69 for a drawing detailing the necessary machining operations for this part. A resulting design consideration with wiring the upper motor was that the hole in the rod could only accommodate one large gauge wire and one signal wire. Therefore, the rod itself served as ground in the circuit. Ground was connected from a bullet connector press-fit into the shelf to the ground on the power distribution board.

Shaft Collars

Shaft collars were used as a way to secure the support tube to the stators of motors, helping to ensure that the tube did not spin (See Figure 19). An off-the-shelf shaft collar was used to support the top motor. However, since this component did not have a matching hole



Figure 18: Final flight vehicle, assembled.

pattern to the motors, an adapter piece was designed so these parts could be connected. A shaft collar mounted to the bottom of the shelf was tightened around the tube, securing the new OX to the vehicle frame. Please reference Appendix Figures 61 & 70, for drawings of the components in the final design.



Figure 19: An off-the-shelf shaft collar, used to mount the upper motor and fix the rod to the vehicle.

Pitch Adjustment Wedges

The gear clamp and lower prop adapter were replaced by the wedge adapter and 3D printed wedges. The wedge adapter was designed with a matching hole pattern to the lower motor (See Appendix Figure 71 for a drawing). The wedges, which were used for additional angle and thrust testing, could be attached to the wedge adapter, as shown in Figure 20. The wedge contained 2 heat-set threaded inserts. The twisted blades could interface directly with these inserts on the wedge. In order to attach the rectangular blades, the rectangular prop adapter would be first attached to the wedges (See Appendix Figure 72 for a drawing). This plate contained two additional holes that would allow the rectangular blades to be

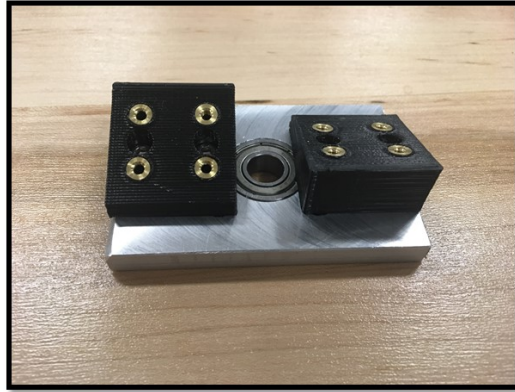


Figure 20: A photograph of angled wedges on the wedge adapter.

secured. From initial tests, we found the gear-clamp system was not an accurate way of securing a blade pitch angle. Sometimes, the angle would change during a test despite all set-screws being securely tightened. Not only did the new angled wedges allow us to more accurately ensure the angle of the lower blade during thrust testing, but they also served as the point of failure during flight tests if the propellers were impacted. These weaker, 3D printed parts were more likely to break than the blades or other structural components. This enabled us to conduct many flight tests without risking breaking the more expensive, but more efficient, twisted blades.

For a labeled overview of the new and final design of the OX sub-assembly, see Figure 21. For a visual of the assembled realization of this design, see Figure 22.

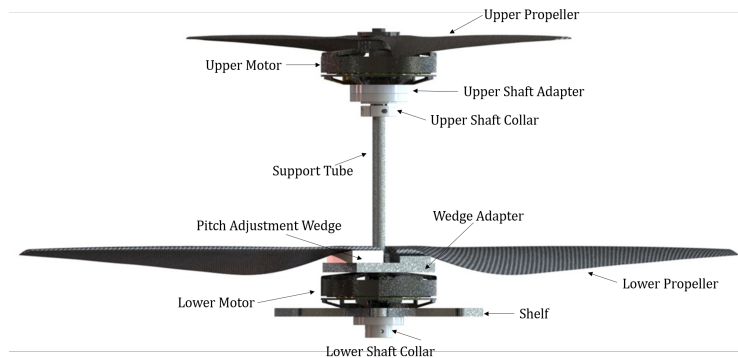


Figure 21: A labeled rendering of the final design for the OX subassembly.

Battery

Finally, during initial thrust testing experiments, it was determined the measured thrust was not significantly greater than the vehicle weight. The total vehicle weight was about 300 grams more than originally estimated. Further, it is likely that additional inefficiencies were introduced with a custom design. First, the rectangular blades, thought to be comparable

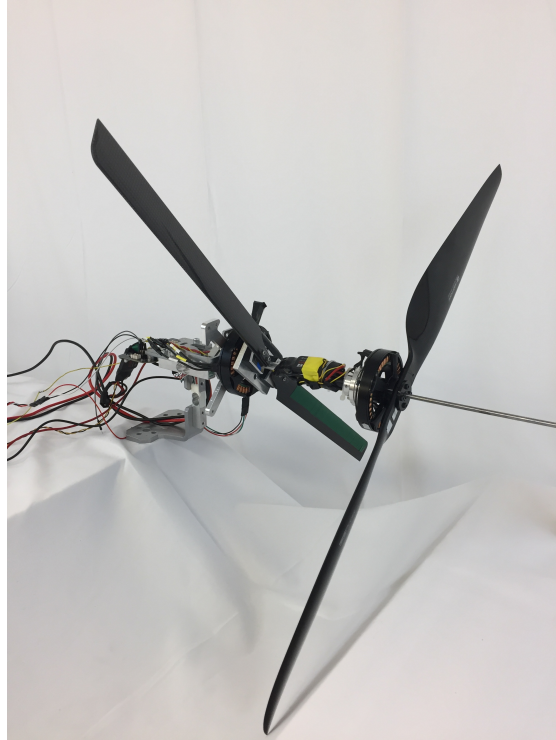


Figure 22: The final design of the contra-rotating system mounted on the thrust stand.

to the twisted blades that were suggested to be paired with the U8 motor, were much less efficient. To be sure that the vehicle could easily get off the ground, a higher voltage battery was selected. This would yield higher RPM for the motors which translates into more overall thrust. In order to avoid adding additional weight with this bigger battery, one with less energy capacity (5000 mAh) was selected, a compromise on total flight time. The 5S battery was ultimately lighter than the original battery, weighing only 727 g [32].

6.4 Quadrotor Subsystem

The quadrotor subsystem is comprised of an off-the-shelf multirotor frame, four brushless DC motors, four propellers, and four custom landing feet. The fully-assembled quadrotor is shown in Figure 23.

6.4.1 Frame Selection

The frame was selected based on the size of the footprint defined by the OX propellers, which were constrained by the width of a doorway. Specifically, the motor to motor distance with the selected frame is 385 mm or about 15".



Figure 23: The quadrotor subsystem, assembled.

6.4.2 Motor and Propeller Selection

The quadrotor was sized using eCalc, an online tool for researchers and hobbyists to select components and specifications of UAVs [33]. The simplifying assumption was that the quadrotor would be responsible for only lifting itself: the frame, 4 motors, and 4 propellers; the rest of the lifting would be done by the OX. Based on this assumption, the vehicle was analyzed in eCalc as though it were a quadrotor with this weight (824g). Based on this analysis, the Antigravity 4004 motors were selected for 10" x 3.3" carbon fiber propellers. See Appendix Figure 73 for a visual of the results.

6.4.3 Landing Gear

Custom feet were designed to support the OXcopter when taking off and landing, shown in Figure 18. To continue to minimize added weight, the feet were 3D printed out of ABS. The feet were mounted to the arms of the frame so they would not interfere with battery and carriage. The feet were designed to be tall enough such that components mounted under the frame would not touch the ground. Hiking pole tips were used on the bottom of the feet for added traction.

6.5 Vending and Carriage

One goal of the Peregrine Parcel delivery system was that the system would not require human interaction. In working towards this goal, the vending and carriage subsystems were designed. While a fully integrated autonomous delivery was not achieved, these subsystems represent early iterations of making autonomous delivery a reality.

6.5.1 Carriage

The carriage was mainly constrained by the type of payload, weight and safety. This payload carrying container was selected as the mechanism to hold the payload over other options, such as a robotic gripper, to ensure that the payload would remain secured in its container should an electronic subsystem fail. A robotic gripper would not be as reliable in this case. Additionally, the carriage could be easily raised and lowered to facilitate deliveries at a distance. This increased safety for humans interacting with our system as the vehicle would not need to fly in the vicinity of humans to make the delivery. Delivery at a distance was achieved via a winch which contained a small geared motor and encoder. Additional safety considerations were made by including a mechanical carriage release mechanism in the form of a snap for the existing prototype. This snap will detach the carriage if a force of around 600g is applied accidentally by the user, preventing the vehicle from crashing as a result.

Our payload was defined to be standard sized candy bars, so the dimensions of the carriage were made to accommodate the range of candy sizes. The size of the carriage was important because if the payload could not be kept in a relatively fixed position within the carriage, it could create instabilities which would interfere with the control of the vehicle. The material of the carriage was selected so that its total mass would be small relative to the defined payload of 300g. Our carriage was made of cardboard, which weighed 28g and met this requirement. In future iterations, other materials and designs could be explored to make this system more robust.

The winch was 3D printed out of ABS for convenience and minimal weight. This was press-fit onto the motor output shaft. Initially, a stepper motor was used for the winch system in order to keep track of the distance the carriage traveled. To accommodate the torque of a 300 g payload at a distance of approximately 5 cm from the shaft (winch diameter), the appropriate motor weighed 110 g. Later, a 9 g Pololu micro-metal geared motor and encoder replaced this stepper, reducing the weight of the carriage system. The encoder counts were inputs to code, which provided the approximate distance that the carriage has been lowered. This way, we could keep track of and control the height to which the carriage was lowered.

A photograph of the final carriage system assembled onto the vehicle and integrated with the vending machine can be seen in Figure 24. The Arduino code used to control the carriage can be found in the final report package.

6.5.2 Vending

The vending subsystem is responsible for housing the off board computer, storing the payload, and dispensing this payload. The design of this system focused on accommodating the carriage, which could be lowered inside. Existing designs of vending machines in combination with the need for a chute for the carriage motivated the design of the first prototype. Thick wires were wound into coils, which were connected to stepper motors via a laser-cut piece of MDF press-fit onto the shaft. This was the mechanism to dispense the candy, which could then fall into the basket. Stepper motors were selected to actuate the number of rotations, so that only one bar would vend at a time. The prototype was fabricated out

of MDF and acrylic, and the size was constrained by the stock sheet dimensions of these materials. This prototype is depicted in Figure 24.



Figure 24: Pictured to the left is the vending machine prototype, and to the right is the final vending machine with OXcopter.

Based on the successful performance of the prototype, the vending machine was redesigned to be large enough for the OXcopter to perch on top. In order to make a sturdy docking station, 80/20 was the selected material. This offered enough design freedom in exchange for convenience. In addition, drawer guides were added to each shelf to accommodate easy stocking of the coils with candy, similar to how commercial vending machines are stocked. The drawers were laser cut and assembled using brackets. The coils were updated to actual vending machine coils, which were cut to the length of the shelves with the assistance of Joseph Valdez. These were attached to the stepper motors via 3D printed adapters, which press fit on both the output shaft of the motor and the coil. In order to increase the reliability of candy landing in the carriage properly, a system of ramps were designed to guide the bars from the shelves. In order to prevent the carriage from getting caught on the shelves as it was being raised, a chute with was positioned in front of the ramps. This chute featured a wide opening to guide the carriage into the proper location. The final assembled vending machine, integrated with the OXcopter and carriage can be seen in Figure 24. A final render of the vending machine in Appendix Figure 74, and the code used to control it can be found in the final report package.

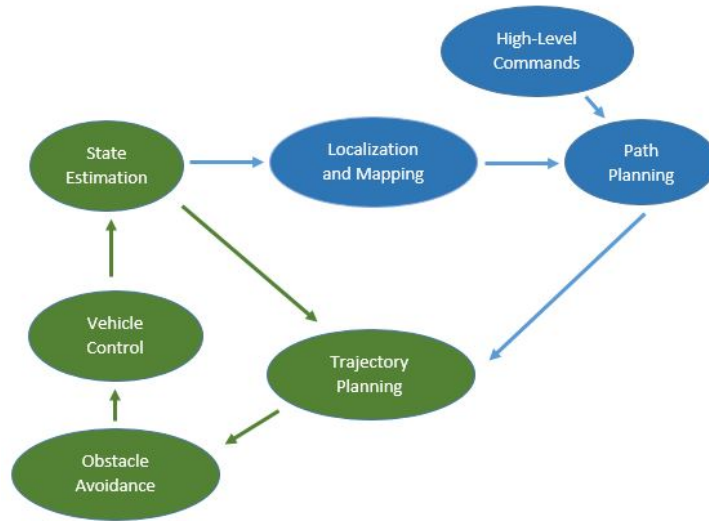


Figure 25: Software architecture for vehicle missions.

6.6 Computation And Electrical Subsystems

6.6.1 System Architecture

In order to complete a successful delivery mission, our vehicle must execute a series of high-level robotic tasks. This sequence will nominally consist of loading an item for delivery, achieving liftoff, flying to the destination, dropping off the payload, flying to a charging station, and docking. In order to complete this sequence of events, the robot must first have a computer-interpretable map of the environment, so that it knows what the building will look like. Then, it must know both its location as well as the location of the target within the building; finding the vehicle's position as it moves is called localization. Once the vehicle is localized, it must generate a basic path throughout the building through a step called path planning, which produces a series of waypoints connected by straight lines that the vehicle can follow to get to the destination. In reality, though, vehicles do not fly straight lines, and the path may intersect obstacles either due to an error in the map or because the environment changes as the vehicle navigates through it. Thus, a second planning step, called trajectory planning, is performed between consecutive pairs of waypoints to generate a collision-free path the vehicle can take. Finally, the trajectory planner outputs commands to the flight controller that is responsible for actuating the motors to maintaining smooth, level flight. The preliminary architecture for the computing system is shown in Figure 25. The green nodes denote calculations done on the vehicle while the blue ones will be done on an off board server.

The robotic tasks we must perform dictate the sensory and compute requirements for our vehicle. State estimation involves both the acquisition of and computation on sensory readings of the surroundings to determine the vehicle's position in the environment. We need the

vehicle to know its current position and velocity to perform flight control as well as localization within a building. For the former, at a minimum, we require a flight controller with an accelerometer and gyroscope data; a compass would be a welcome addition to greatly increase the accuracy of orientation readings. We ended up choosing the Pixhawk flight controller because it has all of these features, including an add-on compass. We also used this particular flight management unit (FMU) because some of our team members, as well as the GRASP laboratory, have experience with the controller, it has much more extensive documentation than other flight controllers, is reliable, and the Robot Operating System (ROS), which we opted to use for reasons described below, already has a large library of code integrating with the device.

6.6.2 SLAM and Path Planning

The localization, mapping, and planning tasks drove both flight controller selection as well as the decision to split computation between an on-board computer and off-board ground stations. Mapping and localization is a very complex problem in robotics; there is an entire field of algorithms called Simultaneous Localization and Mapping (SLAM) being actively researched for this purpose. As such, we chose to look into HectorSLAM, a library contained within the Robot Operating System that has been proven to work. Using ROS, we can easily connect a LiDAR to our device, load an off-the-shelf driver, and then take data from the sensor and feed it into HectorSLAM to generate and save a map of the environment as well as perform SLAM in real-time. Given that our team members are experienced with ROS, ROS simplifies the development of a robotic software system involving many components, and ROS can run between computers over a wireless link, we decided it was the middleware of choice for our system.

After deciding on SLAM as our localization and mapping algorithm, we opted to run SLAM and path planning off-board. These are highly compute-intensive algorithms, and one of the smallest computers capable of running the entire system architecture that can fit on a copter is the Intel NUC line, which many researchers in GRASP use. The NUCi5RYK, the 5th-generation i5 edition, weighs about 1 pound, and the NUCi7RYK, the i7 edition, weighs over 2 pounds [34], [35]. These weights are prohibitively high, however, for a vehicle intended to carry a large payload. By moving the intense computation off of the vehicle itself to a ground station that communicates with the robot, the weight of the computational electronics is no longer critical. The rotor craft will not have to carry these heavy electronics, which means that it is safer, quieter, and has a longer battery life. Most of the heavy computation is contained within the SLAM and path planning subsystems, so we will off-load just these tasks to the ground station. Obstacle avoidance will still be run on-board at a high rate to allow for fast trajectory planning.

6.6.3 Ground Station

The design of a ground station has very few design constraints, other than that it perform SLAM and path planning at a rate of around 1 Hz, which should be sufficient to give a path overview to a vehicle flying at no more than 1 m/s. To this end, we plan to have an Intel

i3 CPU with a GPU performing the heavy-lift computation. The KITTI SLAM benchmark shows that even fast CPUs can only localize and map at a maximum rate of about 10 Hz even when the processor is running only the SLAM program. However, other SLAM benchmarks show that a powerful GPU can update the map far faster [36] [37]. According to SLAMBench, the NVidia Titan GPU can compute slam at 135 Hz using CUDA. This GPU at over \$1000 is cost-prohibitive, but we can likely use the \$120 GTX 1050 Ti to meet our requirements; the 1050 Ti has 1/4 the cores and a lower clock rate than the Titan, so it should run conservatively 10x slower than the Titan, which would still give us a 13.5 Hz SLAM update rate, meaning we have plenty of compute room to run a planning algorithm as well.

6.6.4 LiDAR and Vision Component Selection

In order to determine the bandwidth requirements for a network connecting the ground station and the vehicle, we had to decide upon the LiDAR that would provide scans of the environment to SLAM. Table 7 lists the LiDAR units we considered for our system. We chose the Hokuyo URG-04LX for several reasons. Its low weight and lowest-in-class 2.5W power usage make it suitable for use on a small flying platform. The 240-degree field-of-view, relatively high angular resolution, and 10Hz update rate are enough to perform SLAM at low ground speeds. The 5V input voltage of the device is also convenient, considering that other on-board sensors run will run at 5V, reducing the need for additional power lines.

Both the Velodyne Puck LITE and UTM-30LX are too heavy and prohibitively expensive. The SICK TiM510's angular resolution was unacceptable for indoor use. The URG-04LX-UG01, a cheaper version of our chosen LiDAR, did not offer acceptable measurement accuracy; a measurement error of 3cm at distances of less than 1 meter would put our vehicle at risk of collisions in low-margin areas like door thresholds. The high update rate of the URG04-LX-F01 was simply not needed. Lastly, the RPLiDAR A2, while cheap and perhaps dubiously accurate, was released recently and does not have the reputé or extensive documentation of the Hokuyo series.

For trajectory planning, we also planned to use a stereoscopic depth camera. This way, while the LiDAR provides 2D scans of the environment to SLAM, which computes around 1Hz, we can use the depth camera to get a 3-dimensional picture of the area in front of the vehicle stereoscopic vision and perform trajectory planning at around 30Hz on-board. The craft will utilize the RGBD (Red, Green, Blue, and Distance) data provided by a Asus Xtion PRO as it very similar to the popular Microsoft Kinect but only 0.5 lbs to the Kinect's 3 lbs. This platform is very well-documented and is frequently used for this type of application. At only \$100, the system is readily available and reasonably priced for integration onto our vehicle.

The Hokuyo LiDAR outputs 10 scans a second, each with about 700 bytes of data, for a total of 70 Kb/s that must be transmitted to a ground station. A waypoint list generated from a path planner would be negligibly small, also on the order of kilobytes per second. So, virtually any network should be able to support communication between the vehicle and ground station. We are not allowed to connect robots to AirPennNet, the university's wireless network, so we require a private network for testing. Any antenna we use should be

omnidirectional, since a flying vehicle may not always be in range of a directional antenna; the antenna also needs sufficient range to allow the vehicle to navigate a large area. We chose the Ubiquiti Picostation M2 for these purposes; for around \$70, we get an omnidirectional, high-powered access point capable of communication at 12.5 MB/s over almost a quarter mile that the laboratory some team members work for has documented extensively.

Table 7: LiDAR Selection Table

Name	Freq. [Hz]	Range [mm]	Resolution [deg]	Weight [g]	Accuracy [cm]	Cost [\$]
URG-04LX [38][39]	10	20-4000	0.36	160	1	2000
URG-04LX-F01 [40][41]	35	60-4000	0.36	260	1	2150
URG-04LX-UG01 [42][43]	10	60-3000	0.36	160	1	1115
UTM-30LX [44][45]	40	10-30000	0.36	370	3	5000
RPLidar A2 [46]	10	50-6000	0.9	190	0.05	450
Puck LITE [47][48]	20	10-100000	0.25	590	3	8000
TiM510 [49][50]	15	50-4000	3	150	4	2500

6.6.5 On-Board Processor Selection

The final compute component we selected was the on-board processor that would collect data from the LiDAR and depth camera, transmit LiDAR data over the network to a ground station, perform trajectory planning, and interface with the flight controller and carriage system. This processor thus needs to be light as well powerful enough to run ROS and the software listed above. Wireless is required but does not have to be built onto the chip.

Table 8 shows the microprocessors considered. We decided upon the ODroid XU4. The Gumstix CPUs, while very tiny and low-power, do not have immediate camera support. The BeagleBone Black is under-documented. The TX1, while extremely powerful, is costly and power-intensive. It would also require the development of a custom PCB to interface with microcontrollers and sensors, or would warrant the use of a hefty breakout board. We leave the ODroid as the best option because of its high computing capability. The processor weighs less than 75g, which saves at least 1 pound compared to an Intel NUC-like computer. [34] [35].

6.7 Safety

In addition to the safety considerations in other subsystems, such as the carriage, trajectory planning, obstacle avoidance, and a remote kill switch, a physical safety system adds extra

Table 8: On-board Computer Selection Table

Name	Cost [\$]	Weight [g]	Processor [MHz]	RAM [MB]	Power [W]
ODroid XU4 [51][52]	74	40	A53 @ 2000	2048	10
Raspberry Pi 3 [53][54]	36	60	A8 @ 1200	1024	5
BeagleBone Black [55][56]	57	60	A8 @ 1000	512	5
Gumstix Overo Firestorm [57][58]	159	5.6	A8 @ 800	512	2
Gumstix Duovero Zephyr [59][60]	179	5.6	A9 @ 1000	1024	3
NVidia TX1 [61][62]	415	70	A8 @ 1730	4096	15

protection for people who may be interacting with the OXcopter. The safety system was designed to be lightweight and strong: hoops serving as propeller guards are supported by carbon fiber rods. The full safety system is shown in Figure 26. The following engineering design tables delineate the materials selected for this safety system. There are three key safety components: upper safety hoops, lower safety hoops, and safety support rods.

6.7.1 Upper Safety



Figure 26: A Rendering of the OXcopter with the safety system

Table 9: Upper Safety Hoop: Material Selection

Foam Type	Thickness (in)	Weight of 1 Hoop (g)	Compressive Strength (psi)
Airex C70-40 [63]	0.5	39.653	65
Airex C70-40 [63]	0.25	36.602	65
Divinycell H100 [63]	0.5	51.853	290
Divinycell H100 [63]	0.25	46.516	290

The upper safety hoops serve as propeller guards for the contra-rotating propellers. These hoops are 28" outer diameter and 27.5" inner diameter circular hoops which surround the upper propellers. They are supported by rods which ultimately attach to the shelf. As mentioned, it was desired that the hoops be made of a lightweight material so that they would not add much mass. They should also be strong enough to withstand most collisions. Carbon fiber composite materials were suggested because of their high strength to weight ratio. Also, since these hoops were so large, the sheet materials selected to cut out the custom part needed to be large enough that the hoop could be cut out in one piece, for mechanical simplicity. This limited the carbon fiber composite materials selection to those presented in Table 9. Table 9 demonstrates that the Divinycell H100 Foam Core is much stronger than the Airex Foam Core. Additionally, the 0.5" Divinycell Foam Core will provide more protection without adding significant mass. Thus, the 0.5" Divinycell H100 Carbon Fiber Foam Core was selected for the upper safety hoops. However, due to the high cost of carbon fiber composite materials and an added cost for a custom CNC part, the large safety hoops for the upper propellers were not fabricated. If ordered, the parts would have cost \$715.50 [63]. However, if manufactured on a large scale, this cost could be significantly reduced.

6.8 Lower Safety



Figure 27: A rendering of a lower safety hoop surrounding one of the quadrotor propellers.

The lower safety system consists of four, 10.9" outer diameter, 10.4" inner diameter semicir-

Table 10: Lower Safety Hoop: Material Selection

Foam Type	Total Weight (g)	Total Cost (x4)	Comp. Strength (psi)
Rohacell Fom Core [64]	17.76	\$74.40	217
Airex C70-40 [63]	29.716	\$148	65
Divinycell H100[63]	37.764	\$154	290
Balsa Core [63]	42.1	\$165	1870

cular hoops which surround the quadrotor propellers. This system is shown in more detail in Figure 27. When selecting materials for these hoops, material strength and weight were again high priority. Additionally, since these hoops were much smaller, many more sizes of sheet material could fit the hoops. As a result, cost minimization could enter the equation. Ultimately, as can be seen in Table 10, the Rohacell Foam Core was the lightest and least expensive option without making significant compromises on material strength. As a result, Rohacell Foam Core was used to create the lower safety hoops.

The entire lower safety system was completed and assembled on the vehicle. The Rohacell Foam Core arrived in 5.75” by 11.75” pieces which were individually machined using a ProtoTRAK Mill to create the custom semi-hoops. See Appendix Figure 75 for an engineering drawing and Appendix Figure 76 for an image of the machining process. Afterward, the hoops were attached to their structural supports on the vehicle.

6.9 Support Rods

Table 11: Safety Support Rod: Material Selection

Rod Material	Outer Diameter (in)	Total Weight (g, 4 Rods)	Compressive Strength (psi)
Carbon Fiber [65]	0.156	11	75,000
Carbon Fiber [65]	0.254	36	75,000
Aluminum	0.24	52	35,000
Steel	0.125	91	70,000
Balsa [66][67]	0.188	1	1,754

Safety rods were added in order to support the hoops that were encompassing the propellers. Looking at different materials and sizes, summarized in Table 11, carbon fiber is once again the strongest material for its light weight. Thus, 0.156” outer diameter carbon fiber tubes were selected as the support rods. Additional structural components were used to connect the rods to the hoops and the safety system to the vehicle itself. This components were 3-D printed out of ABS. For example, the rods were attached with connectors which mounted beneath the Antigravity motors. The rods also extended past the propeller to clamp onto the hoops so as to not interfere with propellers spinning during flight. These connectors can be seen in Figure 27. A rendering of the full safety system can be seen in Figure 26.

For more details on the materials selected for the safety system, see Appendix Figure 77.

6.10 System Overview

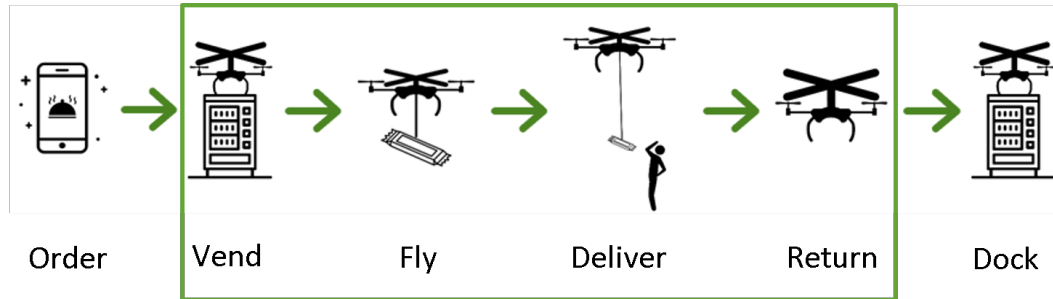


Figure 28: The envisioned steps in our automated delivery system. Scope of the project is highlighted in green.

The final vision for a complete delivery system is as follows, depicted graphically in Figure 28. First, a customer would request their chocolate through an ordering application. Our custom vending machine would then dispense this payload directly into the vehicle which would take off to make the delivery. The vehicle would return to dock back on the vending machine.

As outlined above, the integration of many systems was required to achieve automated vending and autonomous flight. While the entire system is not yet fully integrated, each of the subsystems operates on its own. As Figure 28 shows, we elected to focus on vending and flight due to the large scope of the full project vision. This was achieved through the careful design and selection of the original OXcopter in addition to extensive computational infrastructure and vending capabilities.

See Appendix Table 12 for the final mass bill of the OXcopter. A full bill of materials for the final system can be found in Appendix Tables 13 - 15.

7 Validation and Testing

Considerable effort was dedicated to optimization and validation of the flight vehicle and manifest in the creation and improvement of reliable test setups. Tests began with the commercially available thrust stand by Turnigy shown in Figure 29 and an array of other sensors: a Watt meter to measure the electrical power supplied to the system, tachometers to measure the angular speed of the rotors, an anemometer to measure the wind speed in the wake of the rotors (wash), and a decibel meter to measure the noise from the rotors. For later tests, a thrust stand from RC Benchmark was used because it could also measure torque and the thrust measurements were more reliable. The tests with this equipment were performed by controlling the throttle command to the motors and recording the measurements from

each of the sensors. For safety reasons, the motors were run in an enclosed room and controlled from outside.

7.1 Quadrotor Twisted Blade Test

This test was performed in order to characterize the Antigravity 4004 motors for the quadrotor subassembly with the corresponding 10x3.3 twisted blades. This characterization showed that the quadrotor can provide the necessary thrust to maneuver the vehicle.

7.1.1 Test Procedure

The twisted blades were mounted on the the motors and this assembly was mounted horizontally on the Turnigy thrust stand as shown in Figure 29. The motor was controlled



Figure 29: Antigravity 4004 motor and twisted blade on Turnigy thrust stand

with a microcontroller and Electronic Speed Controller, and for each throttle command the following were measured:

1. Thrust (g)
2. Motor speed (rpm)
3. Noise (dB)
4. Wash (mph)

5. Voltage (V)

6. Current (A)

7.1.2 Results

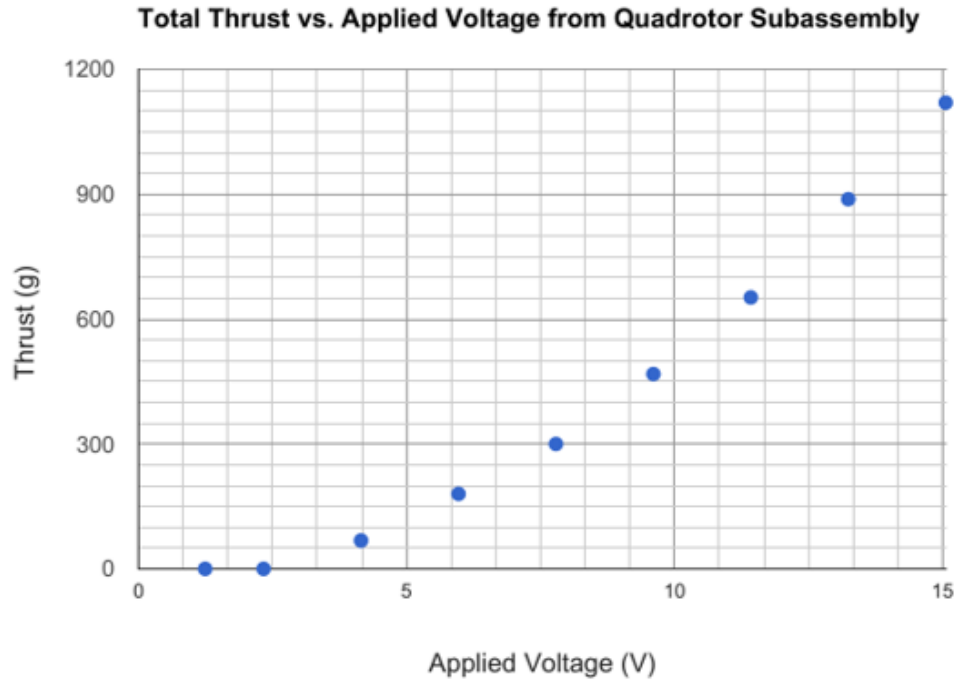


Figure 30: The quadrotor can provide more than enough thrust to lift its own weight of 824g

The results of the tests on the rotors for the quadrotor subassembly are shown in Figure 30 where thrust is plotted against voltage applied. Here, thrust is the total thrust that all four motors would provide at the corresponding voltage, and it was determined by multiplying the thrust measurements obtained from a single motor by 4. The applied voltage was determined by multiplying the total voltage measured by the throttle percentage.

7.1.3 Analysis and Conclusions

The quadrotor was designed to lift only itself: the four motors and propellers plus the vehicle's frame, a total of 824g. Moreover, the quadrotor is tasked with the attitude control of the vehicle, so this subsystem must have a total thrust capacity above the weight it's responsible for in order to properly steer the vehicle. The results bear this out, with the maximum recorded thrust from the quadrotor more than 1.1kg at 15V. It should also be

noted that this experiment was done before the team decided to upgrade from a 4S (14.8V nominal) to a 5S (18.5V nominal) LiPo battery. With the increased voltage, the quadrotor can generate even more thrust.

7.2 Single Blade Tests

To optimize the coaxial rotor system, a number of experiments were required. The analysis began with a single rotor because the upper rotor in the coaxial system was assumed to be independent of the lower rotor. In contrast, the lower rotor operates in the wake of the upper rotor, so its performance is affected by the rotor above it.

These tests were designed to optimize the upper rotor. Many tests were done to determine the optimal blade pitch of the 325mm flat rectangular blades in free air by characterizing the performance of a single rectangular blade across a variety of blade pitches and motor speeds. The test was repeated for 26" x 8.5" hyperbolic twisted blades to compare their performance to that of the rectangular blades.

7.2.1 Test Procedure

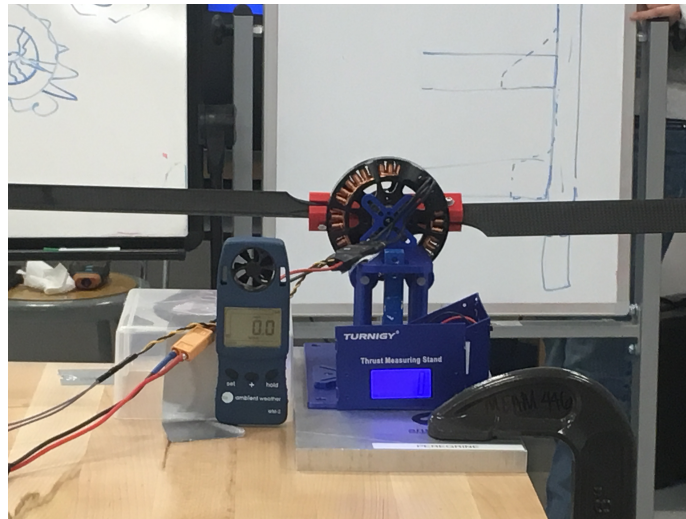


Figure 31: Single rectangular blade test setup

The U8 motor was mounted on the thrust stand, and the rotor blades were mounted to the motor. For the rectangular blades, an aluminum adapter with 3D printed gear clamps (see Design) secured the blades onto the motor. This system, seen in Figure 31, allowed the pitch of the blades to be adjusted before each trial. These steps were followed for a single trial:

1. Set blade pitch angle
2. Measure blade pitch angle using LoggerPro software (Figure 32)
3. Set motor speed by sending throttle command
4. Measure and record:
 - (a) Thrust (g)
 - (b) Angular speed (rpm)
 - (c) Noise (dB)
 - (d) Wash (mph)
 - (e) Voltage (V)
 - (f) Current (A)
5. Repeat steps 3 and 4 for a range of throttle commands

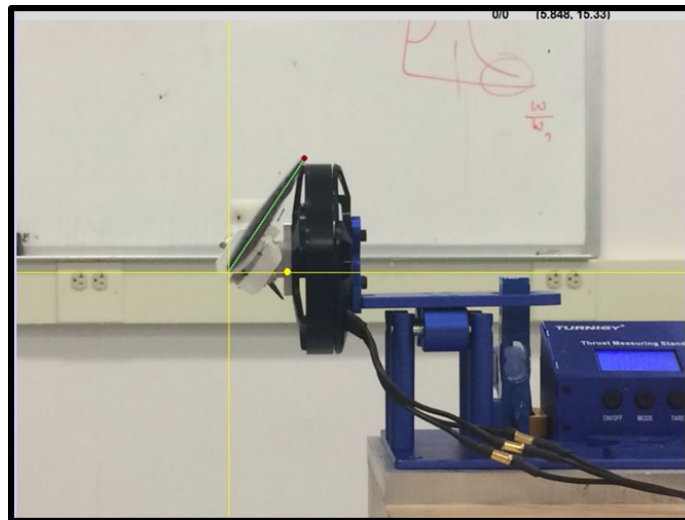


Figure 32: Measurement of the blade pitch angle using LoggerPro

This procedure was then repeated for a variety of angles from 0° to 30° as well as one trial for the twisted blades. Shown in Figure 33, the pitch angle of the twisted blades was not varied because it was assumed to be optimized by the manufacturer.



Figure 33: Single twisted blade test setup

7.2.2 Results

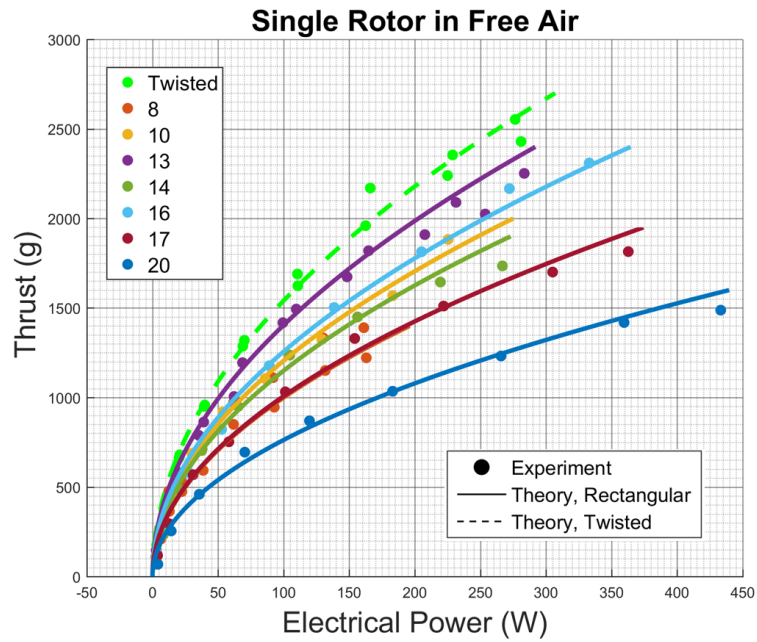


Figure 34: Single rotor in free air

The results of the single blade tests are plotted in Figures 34 and 35. The theory in Figure 34 is fit to the data using motor and blade characteristics derived from these experiments. Figure 35 shows the noise measurements collected by reading a decibel meter 57" downstream from the rotor disk.

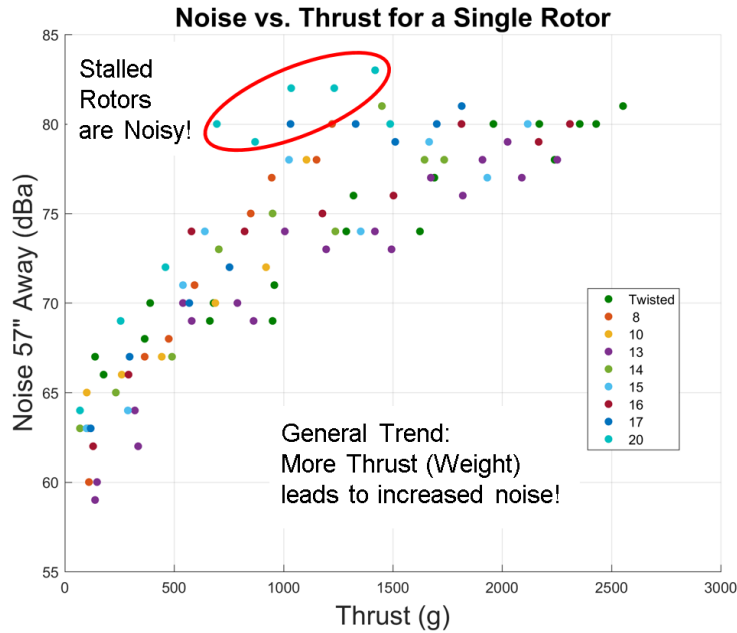


Figure 35: Single blade noise results

7.2.3 Analysis and Conclusions

The experiments indicated that the twisted blade was optimal for the upper rotor of the vehicle. Figure 34 shows how the twisted blade outperforms the rectangular blades at all angles, always getting more thrust for the same input electrical power. More efficient blades also tend to be quieter, and that can be seen in Figure 35 where the twisted blades are among the quietest for a given thrust, followed by the most efficient pitch angles of rectangular blades. As a result of these tests, the twisted blade was selected for the upper rotor.

7.3 Coaxial Rotor Tests

This test was conducted to optimize the coaxial rotor system, considering that the lower rotor operates in the downwash of the upper rotor. To compensate for the increased air flow from the upper rotor, the pitch of the lower rotor should be increased, and these experiments will determine the amount the pitch should be increased.

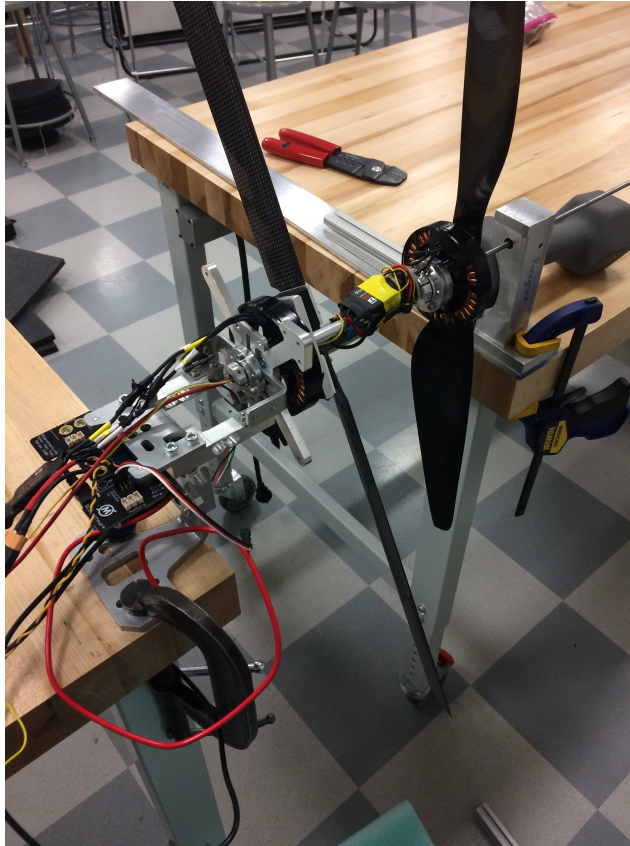


Figure 36: The coaxial rotor system had to be supported on the other end

7.3.1 Test Procedure

The contra-rotating subassembly (the OX) was mounted horizontally on the RC Benchmark thrust stand and was supported on the other side by a linear bearing aligned with the shaft as seen in Figure 36. In these experiments the blade pitch angle was set with 3D printed angled wedges (see Design). Trials followed these steps:

1. Set lower blade pitch
2. Set upper motor speed
3. Vary lower motor speed from 0 to 100%
4. Increase upper motor speed

Steps 2 through 4 were then repeated for upper motor speeds up to 100%. Data were recorded through the use of RC Benchmark's proprietary software.

7.3.2 Results

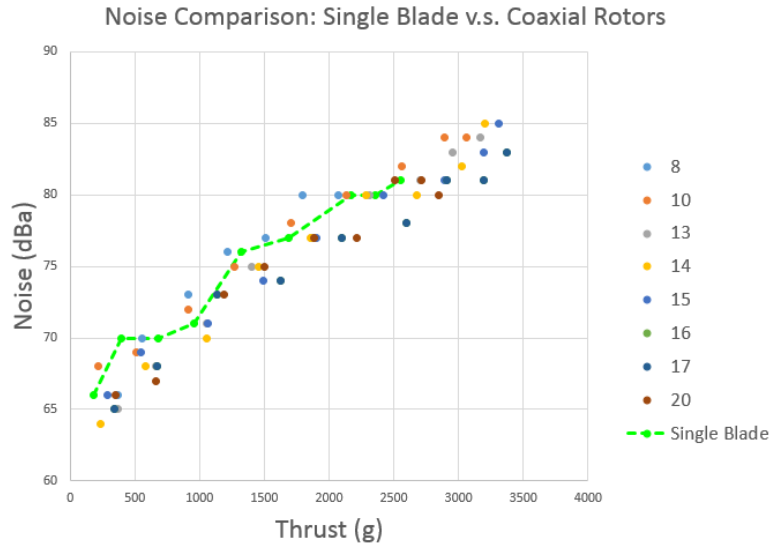


Figure 37: Noise comparison

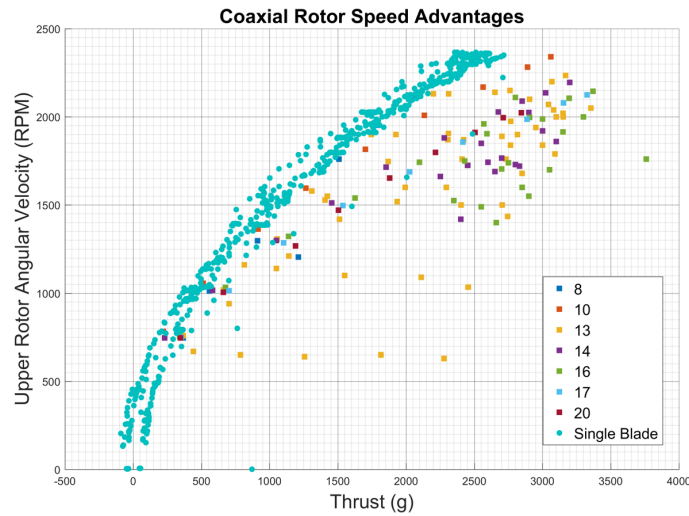


Figure 38: RPM and thrust comparison for single and double twisted blades

Figure 37 is a plot of the noise generated by the OX 57” downstream from the lower rotor, measured with a decibel meter, compared to the same measurements of a single rotor. Figure 38 shows the angular speed in revolutions per minute that the blades have spin to generate

a certain thrust at various pitch increases and compares this to the results for a single rotor.

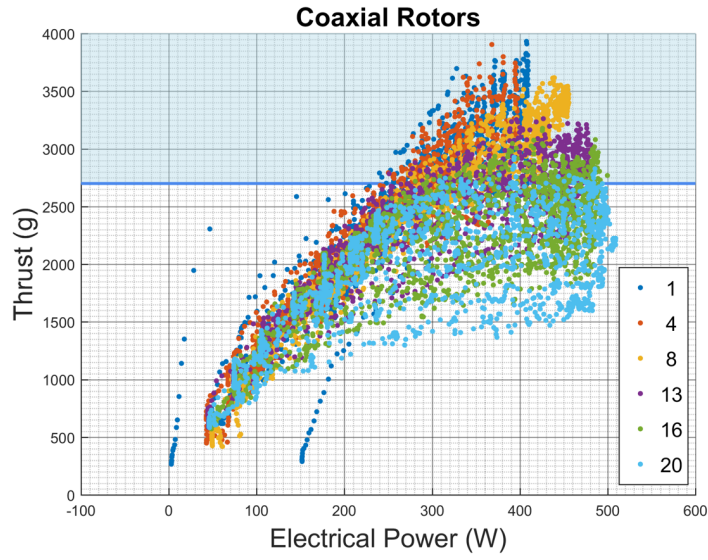


Figure 39: Double twisted blade thrust results

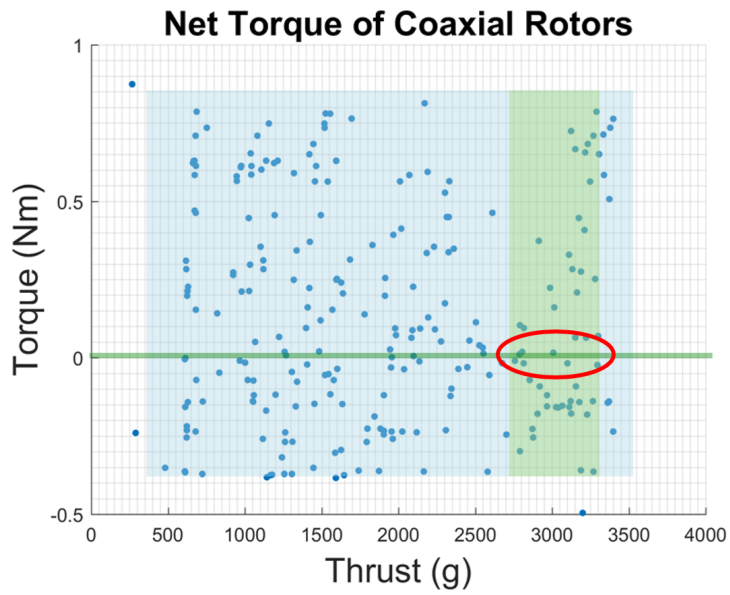


Figure 40: Double twisted blade torque results

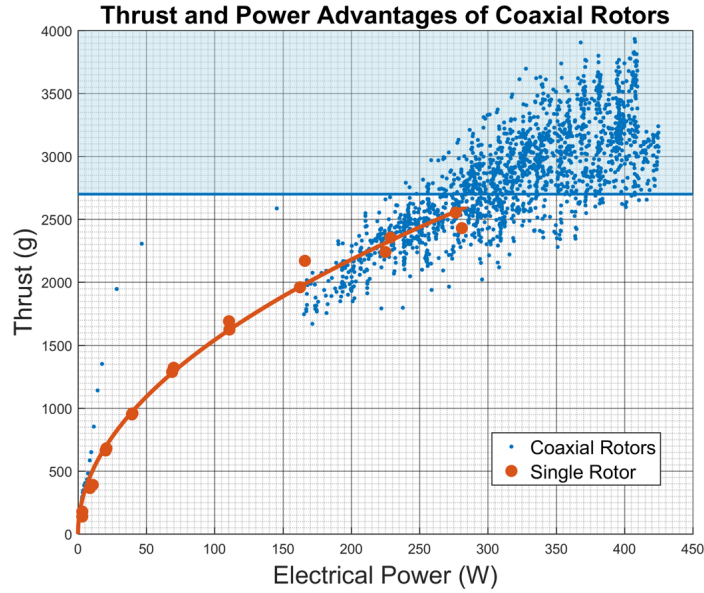


Figure 41: Thrust and power advantages of coaxial rotors

Figure 39 plots the results of the coaxial rotor tests for two sets of twisted blades with the lower rotor at various angles of incline. The optimal angle, 1° , can be seen to provide more thrust for the same input electrical power than the other angles. The torque measurements for this angle are plotted in Figure 40, showing the range of thrust/torque combinations that can be achieved by the contra-rotating propellers. The balance (0 Nm) torque condition and the viable operating range (2700g - 3300g of thrust) are highlighted in green, and the data show that these conditions can be met by the system. Finally, Figure 41 demonstrates the advantages of the optimal configuration of coaxial rotors compared to the results of a single rotor.

7.3.3 Analysis and Conclusions

These experiments led to several important results. First, it can be seen in Figure 37 that, for a given thrust, adding the second rotor does not make the vehicle any noisier. Moreover, from Figure 38, the blades in the coaxial system can spin slower compared to a single rotor and generate the same thrust. Since angular speed is related to power, this result confirms the power advantages expected from coaxial rotors.

As shown in Figure 39, inclining the lower blade negatively impacted performance, with lower inclines generating more thrust for the same input electrical power. This result ran counter to our intuition and that of our advisers. Nevertheless, based on the experimental results, the lower rotor was not inclined for the final flight vehicle configuration.

The results of our torque data, shown in Figure 40, show that for the optimal lower blade

angle (no incline) the torques can be balanced while enough thrust to fly is generated. This confirms the viability of the flight vehicle.

Within our operating range the coaxial rotor configuration has efficiency advantages over a single rotor, according to Figure 41. There are two important results. First, the single rotor could not provide the thrust needed to fly the vehicle, so a heavier battery would be required for a vehicle to be viable with just a single large rotor. Secondly, in the flight condition, the coaxial system outperforms the single rotor, generating more thrust for the same input power. These results confirm the advantages of the OXcopter design and validate the team's claims to greater efficiency and lower disruptiveness.

7.4 Flight Tests

With an optimized flight vehicle, hover tests came next (Figure 42). The vehicle was able to achieve a degree of stability in flight several times, but it is not yet reliable since tuning the gains for this unique multirotor took much longer than anticipated. See the final report package to view videos of flight tests.



Figure 42: Team Peregrine prepares for a hover test

7.5 Computation Validation

7.5.1 LiDAR Testing

In the fall, experiments were conducted to determine how the selected LiDAR, the Hokoyu URG-04LX, would perform in the field. To test the range accuracy of the LiDAR on various materials over a range of distances, the LiDAR was fastened to one end of a workbench with a tape measure running the length of the table. This also allowed our testing location to be repeatable. For non-reflective materials, like wood, cardboard, and plaster (the wall), the LiDAR had an accuracy of $\pm 5mm$. However for more reflective surfaces, like metals, and shiny plastics, the system tended to over predict by up to $5cm$.



Figure 43: LiDAR testing setup

7.5.2 HectorSLAM Testing

Full validation of the localization capabilities of our system would have required testing on the OXCopter platform. However, that system was in the tuning process so a small wooden cart was used instead. This allowed us to watch as the algorithm generated the map around its current location in real time. After successfully mapping the 3rd floor of Moore, we considered this subsystem to be complete and ready to test on the robot after the tuning process.

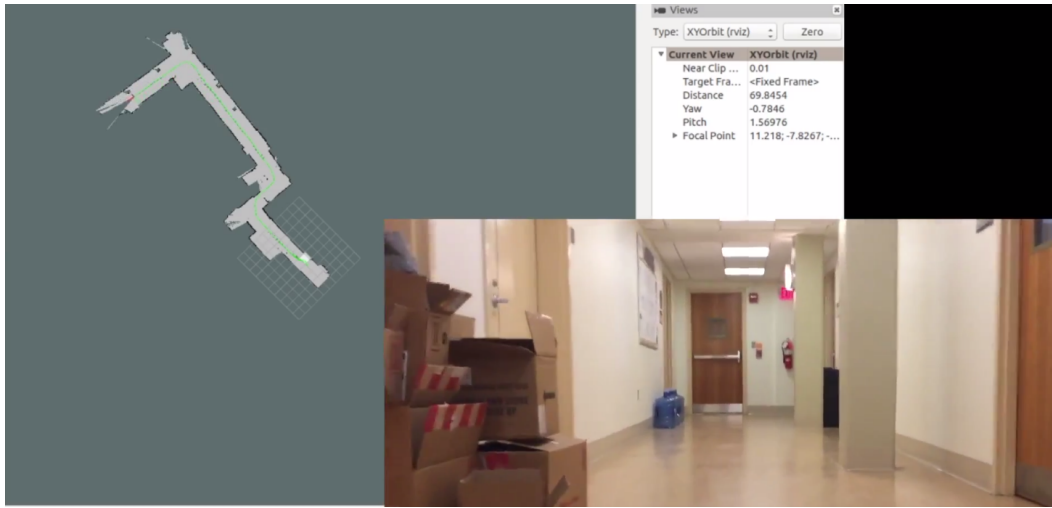


Figure 44: SLAM Validation

7.5.3 Wireless Testing

To transmit the sensory data to the base station for processing we selected the Ubiquiti Picostation M2 to be as our wireless way-point. However, we ran into problems setting up the Picostation and ran out of time to fully debug the issue. Thus, in order to test the base station's capabilities, we connected both the base computer and ODroid to a mobile hotspot, emulating how the system would have been set up had the Picostation been operational. This allowed us to configure the ROS environment running on the ODroid to directly transmit the data to the ROS environment on the larger computer completing our goal.

7.6 Carriage and Vending Machine

The vending machine and carriage (Figure 45) have been shown to work as an integrated unit. The vending machine's coils vend the candy, and a system ramps reliably guides the candy bars to the carriage. The carriage is then raised up by a winch for takeoff. See the final report package to view videos of the system working.

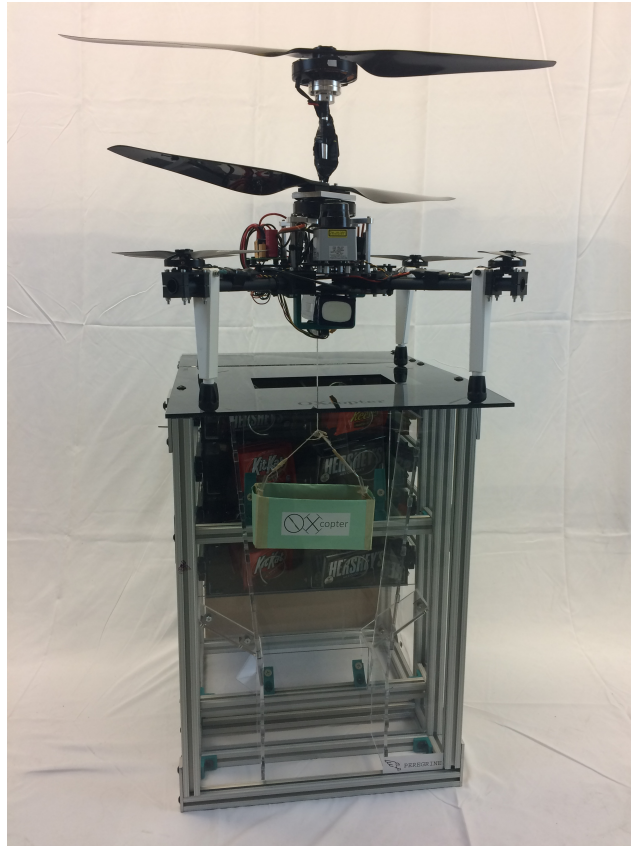


Figure 45: The ramps of the vending machine guide candy into the winch-actuated carriage

8 Discussion

8.1 Target versus Accomplished Performance

8.1.1 Flight System

In the Fall we set out to build an aircraft capable of stable hover with an artificial payload and we fell short of this goal. Our original plans involved retrofitting an off-the-shelf rotor system for the task but in order to increase our efficiency we turned to a completely unique design. This decision to design from the ground up lead to several setbacks that we did not anticipate, such as vibrational shaft issues and difficulty tuning. Despite these troubles, our experiments showed that we were able to achieve the conditions necessary for lift although the time constraints of this course prevented us from fully tuning the vehicle.

8.1.2 Dispensing System

As part of our goal of a fully autonomous system, we designed the OXcopter to be able to load a package without human interaction. This involved a lower-able carriage that we aimed to make less than 100 grams. We far surpassed this goal by designing this subsystem to be only 28 grams while isolating the vehicle above with a safety quick release if too great a force is exerted on the carriage.

We also designed a custom vending machine that would act as home base for the OXcopter. The vending system was configured to dispense the requested candy bars into the carriage. We only achieved our intermediate goal of minimal human interaction with this component as we were able to successfully vend a candy bar into the carriage but it required a human to press a button located on the back of the machine.

8.1.3 Computation System

We were able to demonstrate the reach goals of our computation system off the vehicle as we did not have a vehicle capable of stable flight in time. This included a working implementation of a SLAM algorithm (Simultaneous Localization And Mapping) that allowed the vehicle to localize itself within a map. We were also able to take this sensor data and stream it wirelessly to our base station computer, allowing it to perform these computations faster by using a larger graphics card than one that could be carried by the vehicle. While we had set no explicit target for the path planning algorithm it was left in the debugging stage as most efforts were spent on tuning in the final days of the course.

8.1.4 Safety

For the safety system we reached our intermediate goal of designing a passive subsystem for the OXcopter. This was a cage that isolated the blades a from directly contacting foreign objects in the environment. We did fall short of our reach goal which was to implement an active object avoidance system into the path planning but we ran out of time to tackle this problem as it required a flying vehicle to test.

8.2 Recommendations

8.2.1 Lessons Learned

Throughout the course of the project several invaluable lessons were learned that should be taken to heart if further work on a related system were to occur. First and foremost with such a large project scope organization was incredibly important. At the beginning of the project our organizational efforts were concentrated in weekly cleanups. Once the project expanded into multiple rooms, with separate designing and testing areas, allocating resources into a storage cabinet for our tools and components sped up our work flow considerably. We

learned that starting with proper storage for tools and components, and keeping with an organization scheme will help move the project forward with less friction.

Another important factor to the momentum of the project was having the right tools for the job. We struggled for several months to get a cheap thrust stand to measure accurately and consistently with our set up. It wasn't until we bought a more expensive and higher quality thrust stand that we were able to generate reliable data. We would have saved a lot of time and anguish if we had purchased the better thrust stand earlier.

8.2.2 Future Work

The future vision for this project requires efforts that were out of the scope of MEAM Senior Design due to the time and funds available. Tuning of the final flight vehicle was challenging and time consuming and due to the time constraints of the course was not accomplished. A more methodical approach to tuning would decrease the time required to get the vehicle off the ground. A rig designed to hold the vehicle about a pivot point would allow for tuning of the parameters separately instead of all at once. This rig would need to be designed and built, but would greatly assist in getting the vehicle off the ground in a stable manner.

We would like to claim that our vehicle is more efficient for carrying payloads than a standard quadrotor or hexacopter. However, in order to verify this claim our vehicle should be compared to a similar quadrotor or hexacopter with the same footprint, weight, and actuator mass. Future work would involve building this comparison vehicle and testing it similar to the tests performed for the OXcopter.

The envisioned use of our vehicle requires operation around people. In order to ensure the safety of those around the vehicle, rigorous testing of the passive, and eventually active, safety system is required. The strength of the carbon fiber hoops and their deflection should be characterized. Adding the additional weight distributed along the safety system could affect the flight dynamics, and some parameters may need to be re-tuned.

9 Budget, Donations, and Resources

9.1 Funds Received

Team Peregrine would like to thank all those that contributed financially to this project including the MEAM Department who generously allocated \$2,520 to this project and the Hershey Company who generously contributed \$10,000 to this project. Peregrine would also like to thank ModLab for donating a Pixhawk PX4 flight controller, which would have cost around \$100.

9.2 Expenses

Description	Cost	Purpose
ODROID-XU4 onboard processor and accessories	\$99.50	Final prototype
Hokoyu LiDar Laser Rangefinder	\$1,935.00	Final prototype
ASUS RGBD Sensor	\$137.12	Final prototype
QUADframe vehicle frame	\$105.00	Final prototype
Antigravity 4004 motors	\$291.80	Final prototype
10" x 3.3" propellers	\$51.80	Final prototype
U8 Motors	\$559.80	Final prototype
26" x 8.5" Propellers	\$235.90	Final prototype
Electronic Speed Controllers	\$185	Final prototype
5S 5Ah LiPo Battery	\$63.89	Final prototype
5V Regulator and Power Distribution Board	\$134.97	Final prototype
Remote killswitch and Power Distribution Board	\$361.57	Final prototype
Electronic components	\$232.23	Final prototype
Carriage parts	\$60.73	Final prototype
Safety system components	\$109.18	Final prototype
Structural components	\$56.99	Final prototype
Vending machine components	\$542.46	Final prototype
Ubiquiti Wireless Access Point	\$81.89	Computer components
Offboard server	\$554.66	Computer components
325mm carbon fiber rectangular blades	\$89.97	Preliminary prototypes
Rotary shafts and bearings	\$188.48	Preliminary prototypes
Bevel gears	\$45.02	Preliminary prototypes
4S 10Ah LiPo Battery	\$72.35	Preliminary prototypes
Carriage parts	\$27.85	Preliminary prototypes
Safety prototyping materials	\$85.19	Preliminary prototypes
Extra prototyping materials	\$141.41	Preliminary prototypes
Electronic Speed Controllers	\$31.98	Preliminary prototypes
U8 and Antigravity 4004 motors	\$851.60	Purchasing error by business office
Duplicate order	\$49.51	Purchasing error by business office
Turnigy thrust stand	\$60	Testing equipment
Quantum 8-channel RC Transmitter	\$70	Testing equipment
LiPo Battery Charger	\$71.44	Testing equipment
Tachometer	\$31.75	Testing equipment
Decibel meter	\$20	Testing equipment
RC Benchmark thrust stand	\$549.66	Testing equipment
Fasteners, etc.	\$210.83	Tools and supplies
Electrical and computer supplies	\$219.45	Tools and supplies
Tools and stock	\$149.92	Tools and supplies
Miscellaneous tools and supplies	\$293.47	Tools and supplies
Spare motors, propellers, and ESCs	\$491.68	Spare components
Spare battery	\$63.89	Spare components
Spare vending machine components	\$12.99	Spare components
Spare rotor blades	\$769.98	Spare components
Spare shaft collars	\$138.19	Spare components
Miscellaneous spare components	\$99.57	Spare components

9.3 Resources and Facilities

9.3.1 Manufacturing and Prototyping

For the manufacturing of prototypes and custom test setups, Peregrine used the MEAM labs and the resources available therein including:

- Senior Design Lab, for assembly
- Rapid Prototyping Lab, for laser cutting
- Precision Machining Lab, for machining
- AddLab & satellite printers, for 3-D printing

9.3.2 Experiments and Testing

Peregrine conducted many thrust tests and rotor experiments in MEAM's Aerodynamic Testing Lab in B2 (Appendix Figure 78) as well as preliminary hover tests. Extensive hover tests were conducted in a small room in Moore 300 (Appendix Figure 79) and some of them outside on Shoemaker Green.

A Appendix



Figure 46: A stadium is an example of a chaotic environment [68].



Figure 47: An airport is an example of a chaotic environment [69].

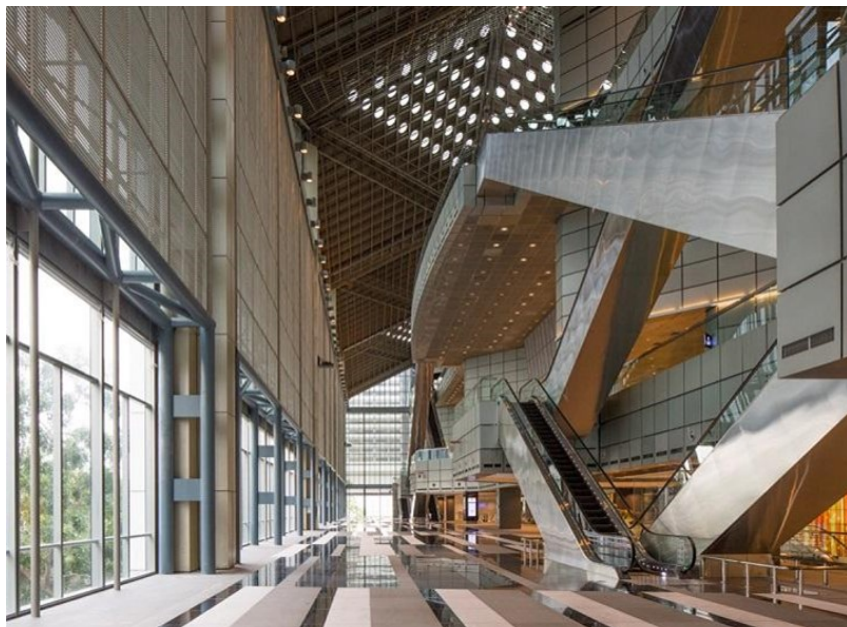


Figure 48: A convention hall is an example of a chaotic environment [70].



Figure 49: A factory is an example of a chaotic environment [71].

Clear Width and Vertical Clearance of Doors and Gates [§404.2.3]

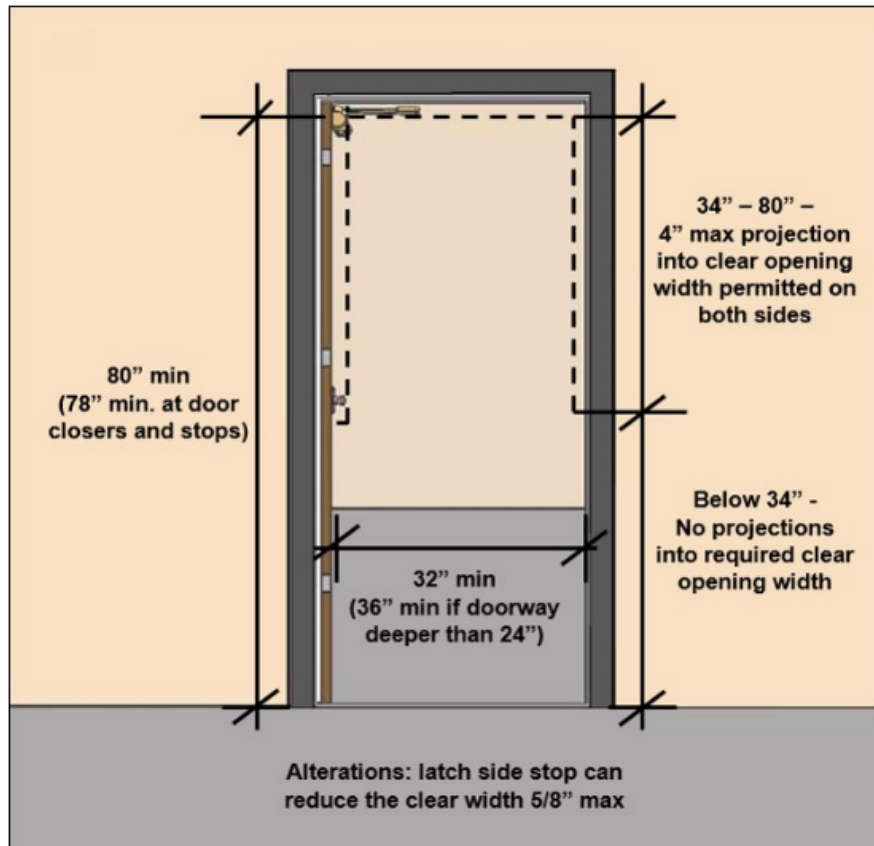


Figure 50: United States Access Board doorway standards [20].

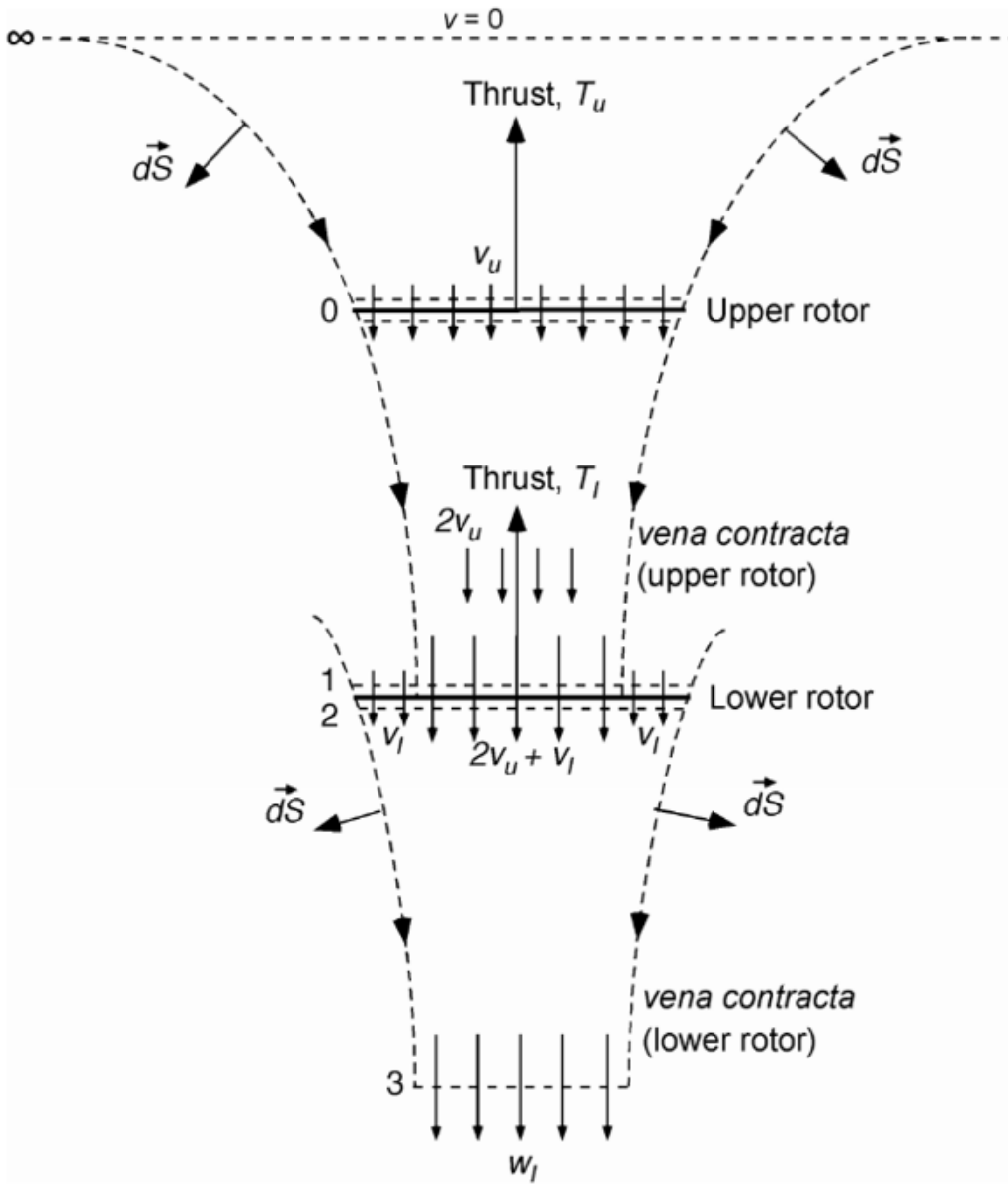


Figure 51: Flow visualization for a coaxial rotor system [18]

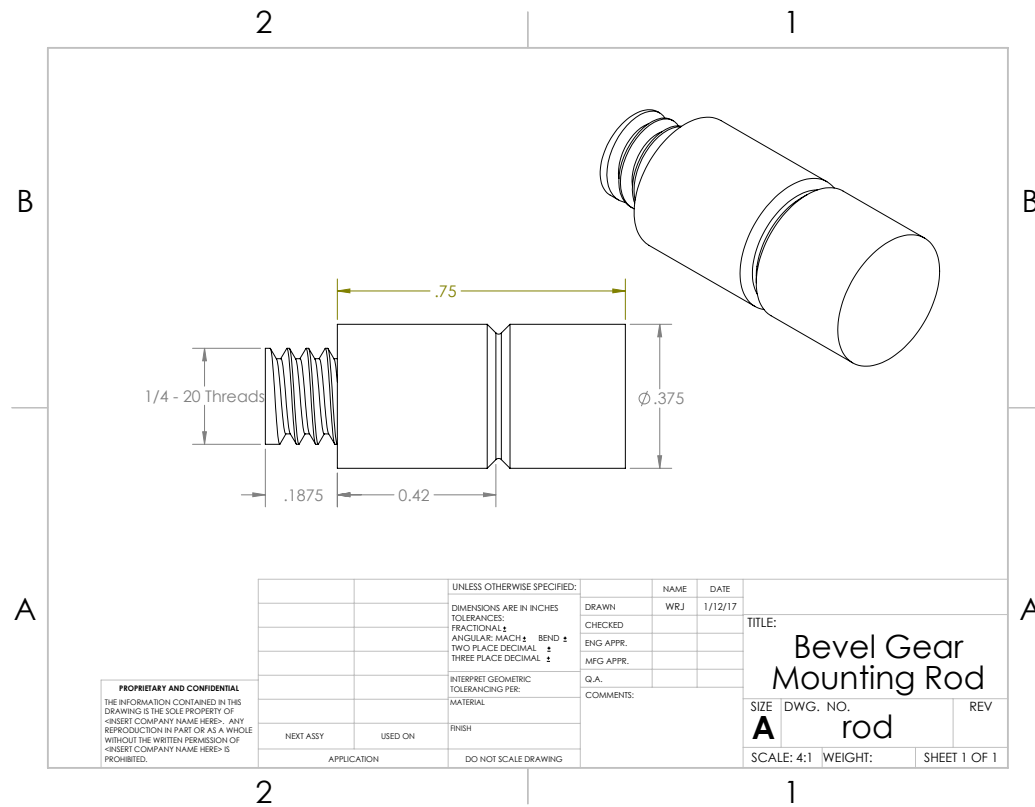


Figure 52: Rods for supporting gear-clamps (from first prototype)

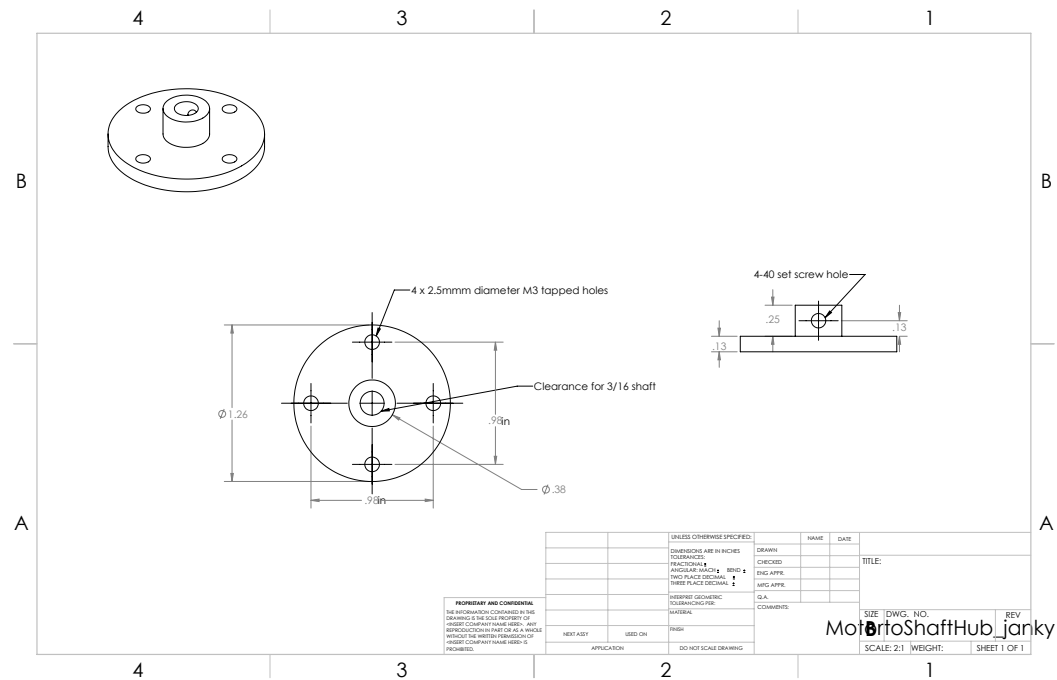


Figure 53: Hub used to transmit motion of the lower motor to the rotating shaft (from first prototype).

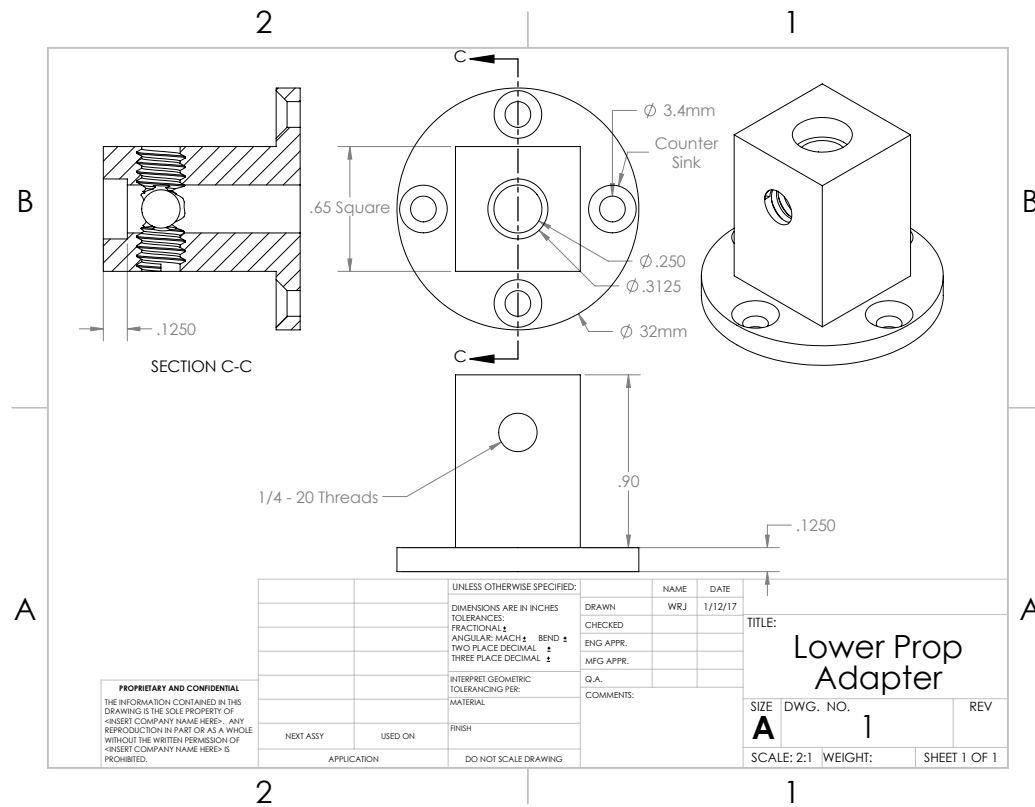


Figure 54: Lower propeller adapter (from first prototype)

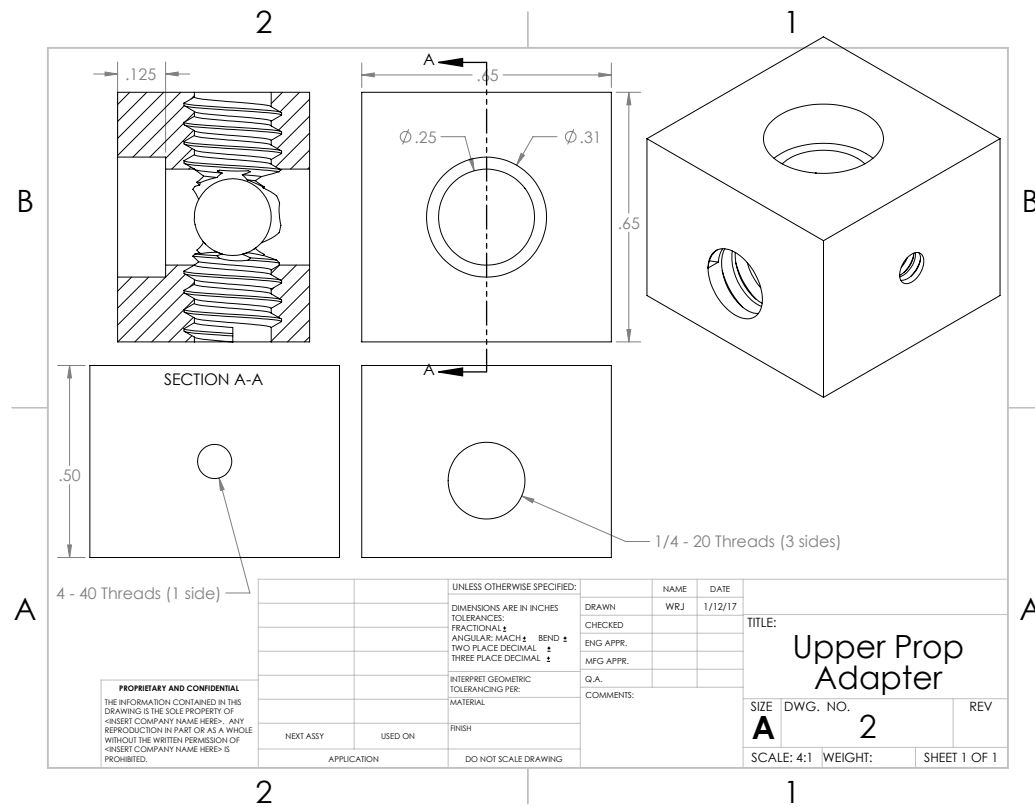


Figure 55: Upper propeller adapter(from first prototype)

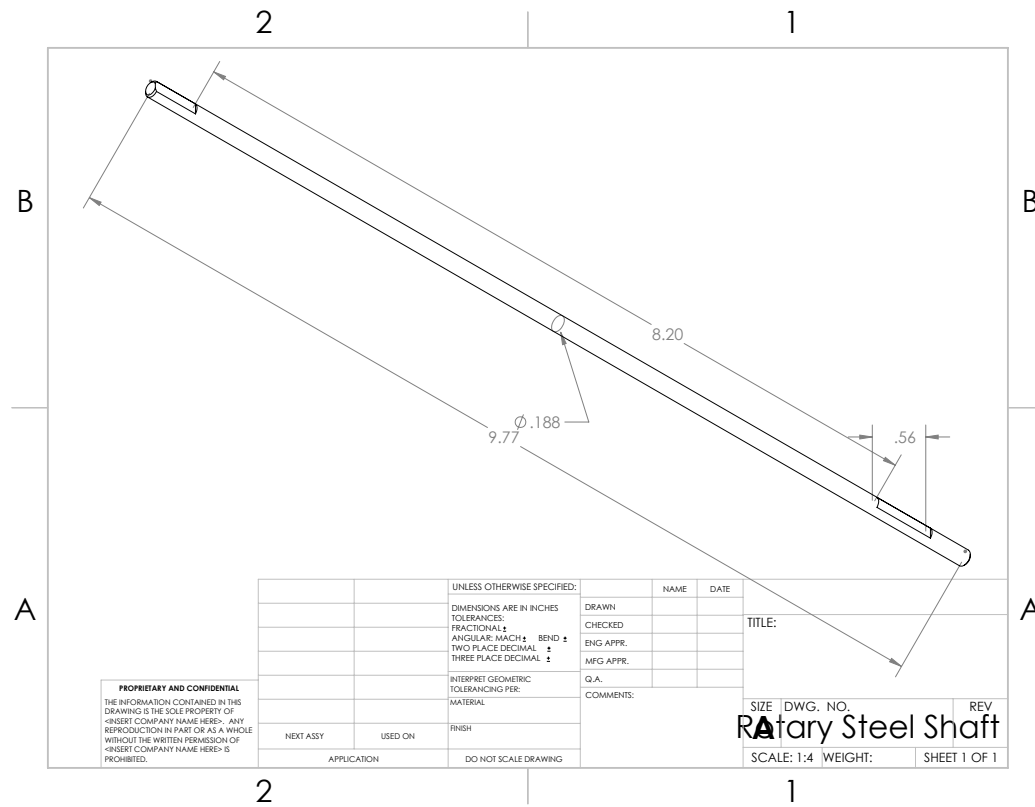


Figure 56: Rotary shaft (from first prototype)

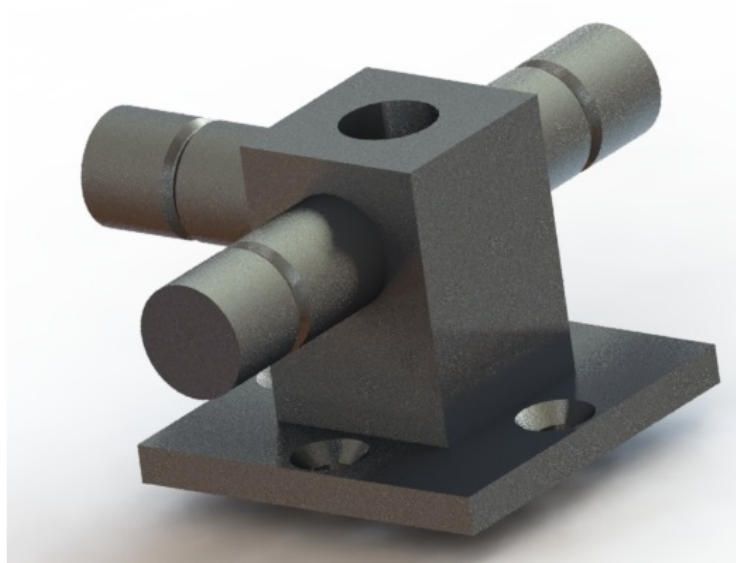


Figure 57: Lower propeller mount with rods (from first prototype).

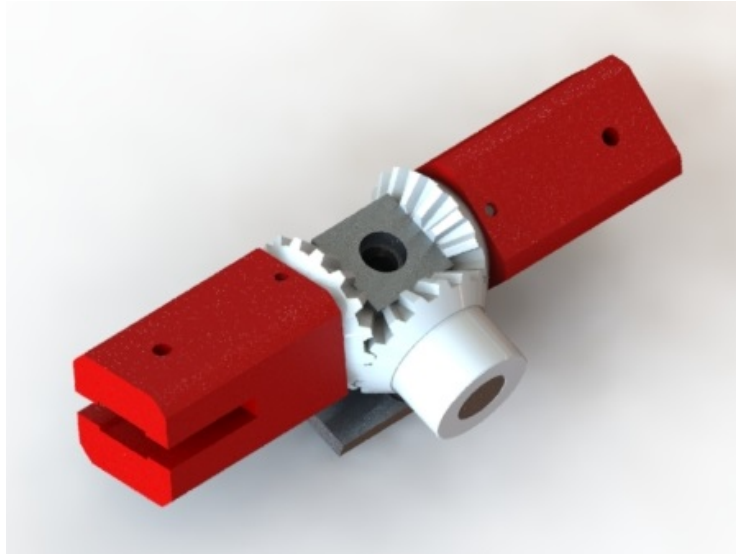


Figure 58: Lower propeller mount with rods and clamps (from first prototype).



Figure 59: Upper propeller mount with rods (from first prototype).

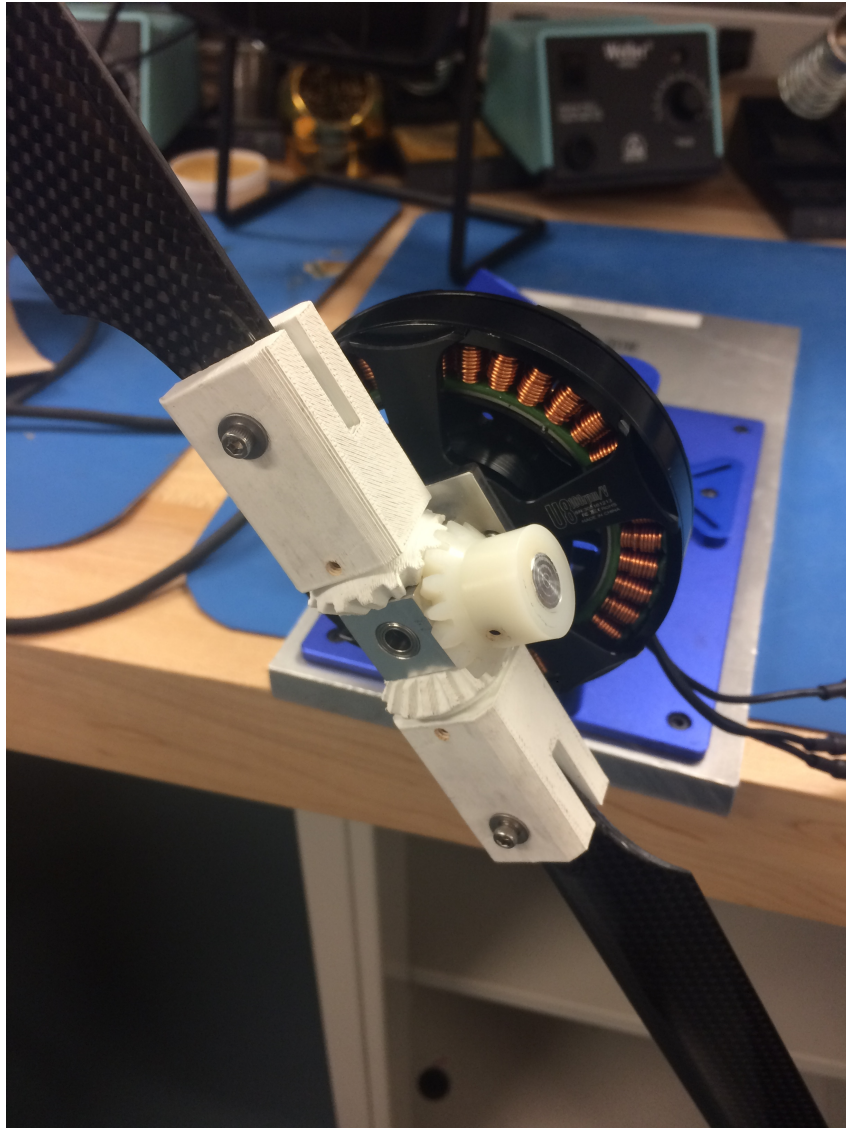


Figure 60: A front view of the first prototype of the rotor pitch adjustment mechanism, assembled.

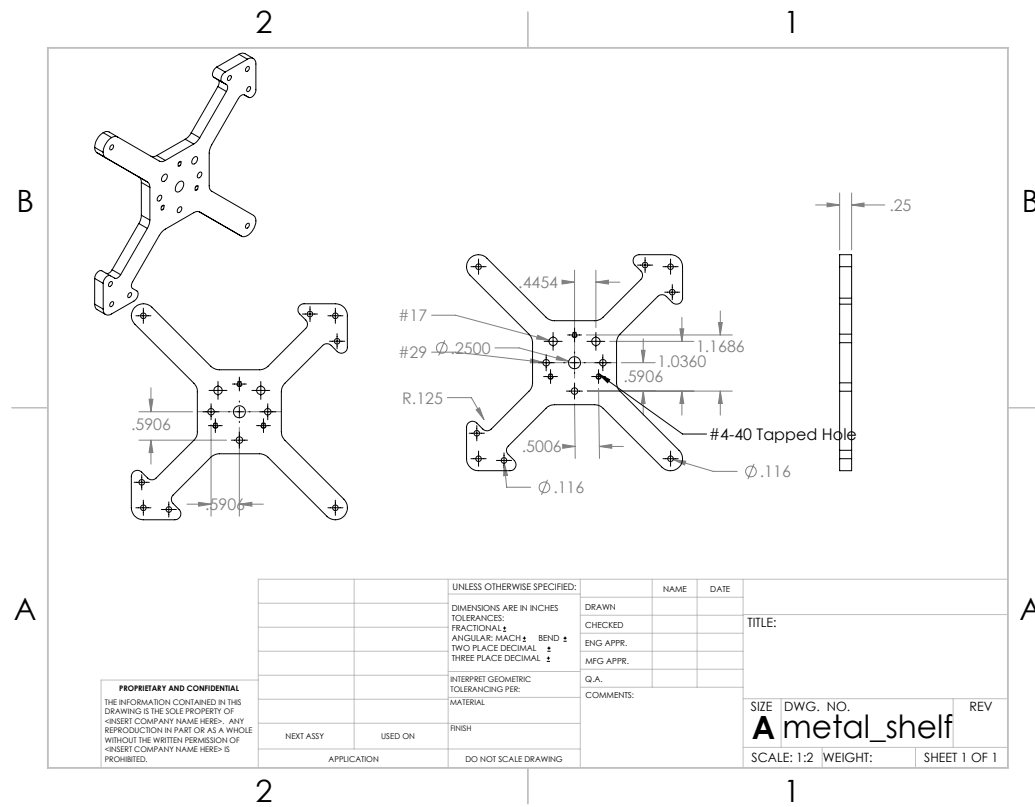


Figure 61: Metal shelf

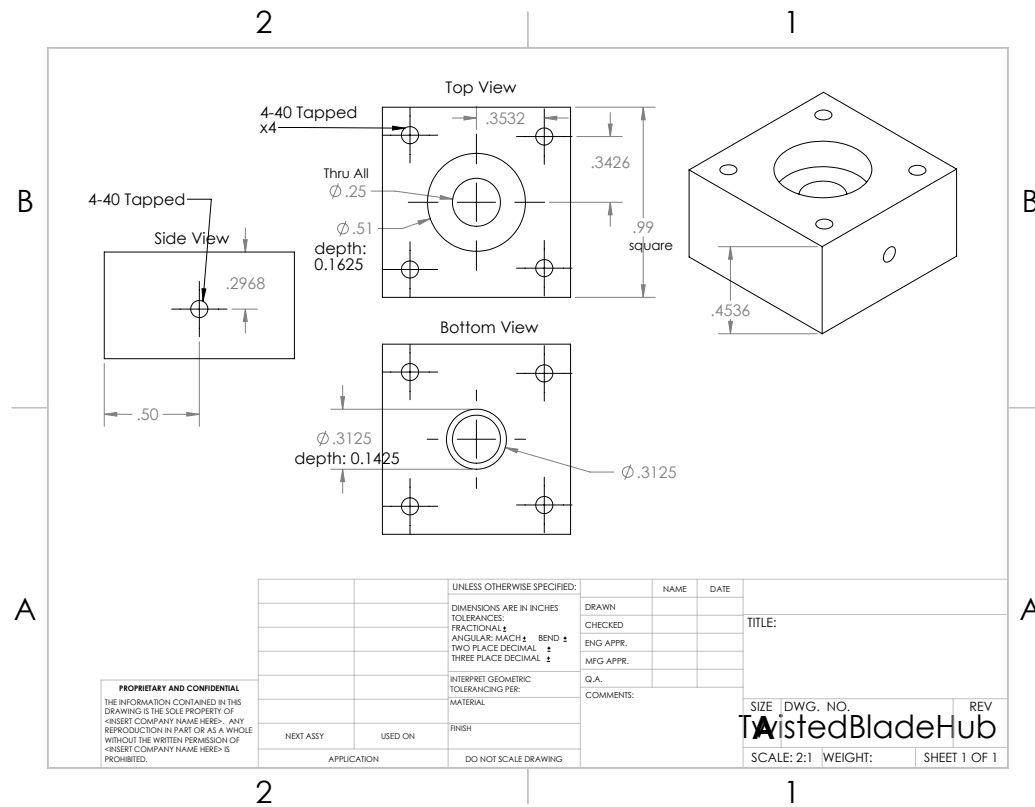


Figure 62: Custom hub for attaching the twisted blades to the shaft

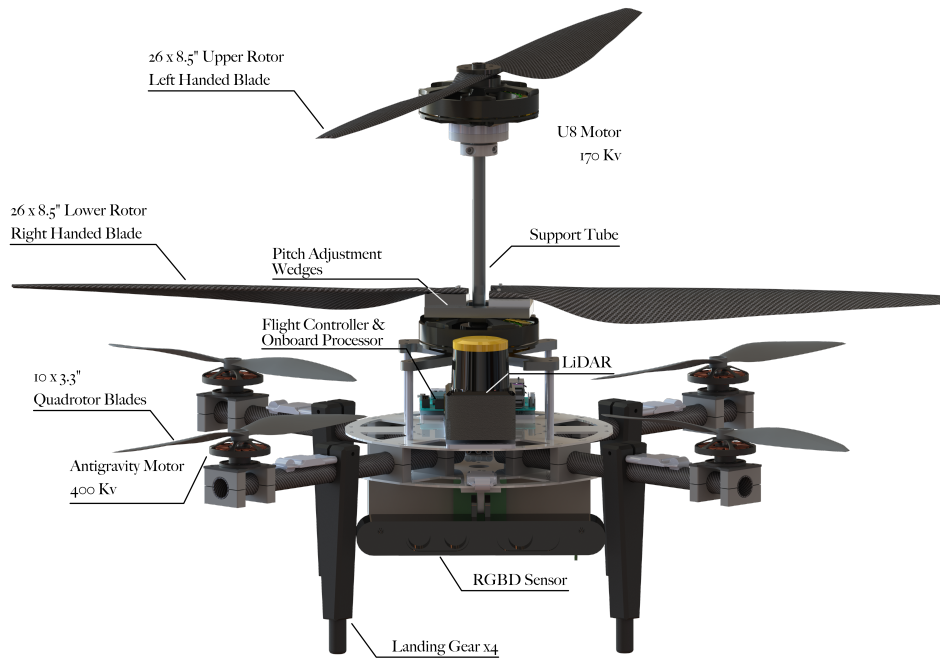


Figure 63: A labeled rendering of the final full flight vehicle



Figure 64: Final flight vehicle.

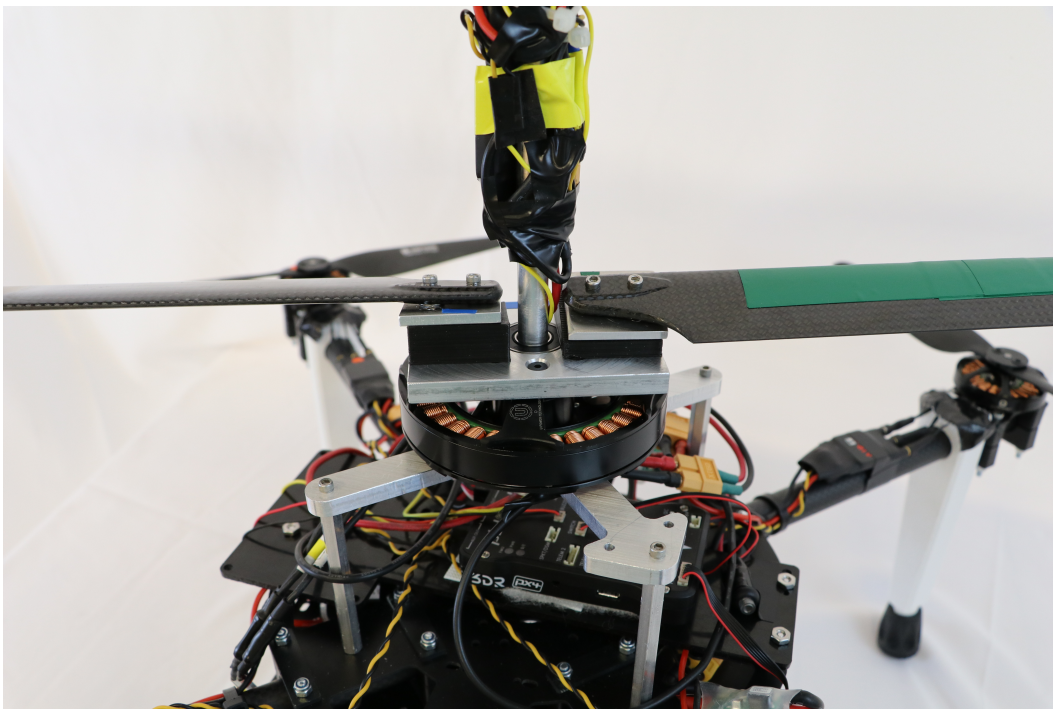


Figure 65: Final flight vehicle



Figure 66: Final flight vehicle



Figure 67: Final flight vehicle



Figure 68: Final flight vehicle

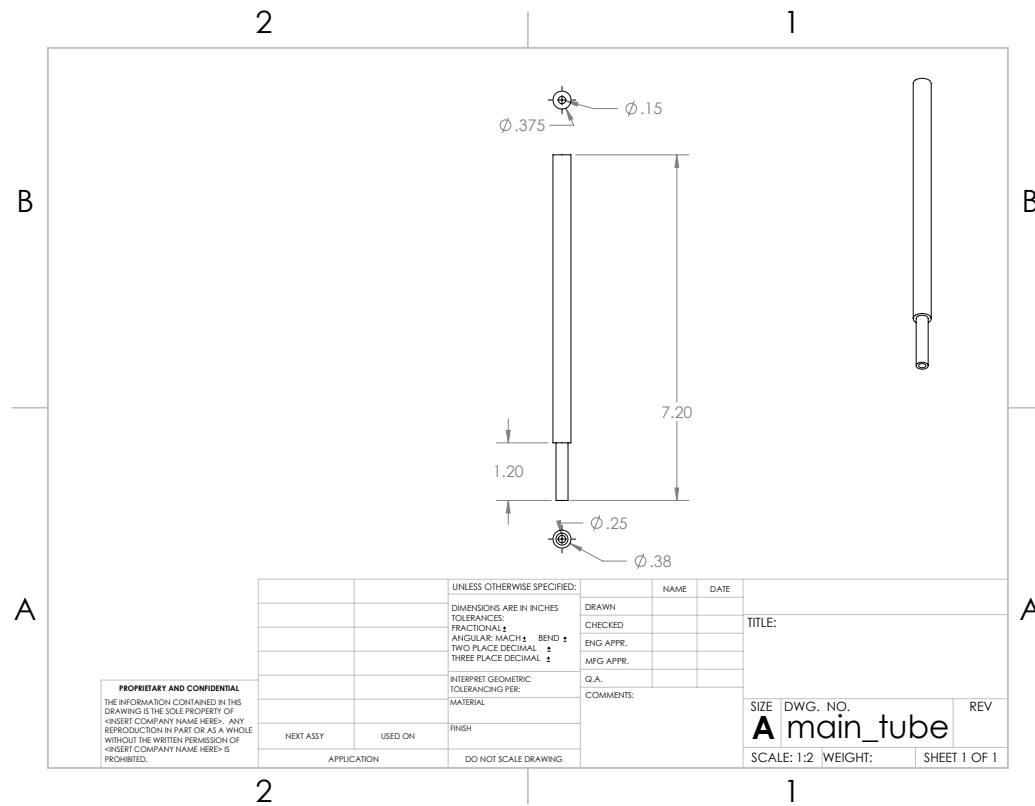


Figure 69: Central support tube

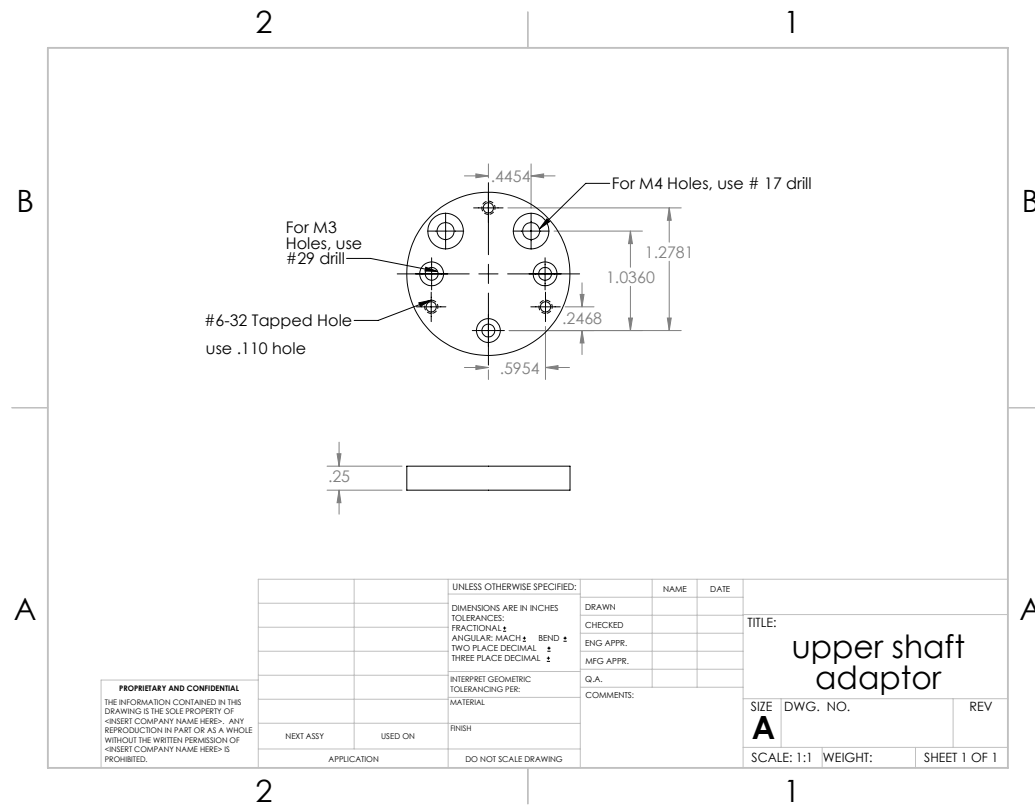


Figure 70: Upper shaft adaptor

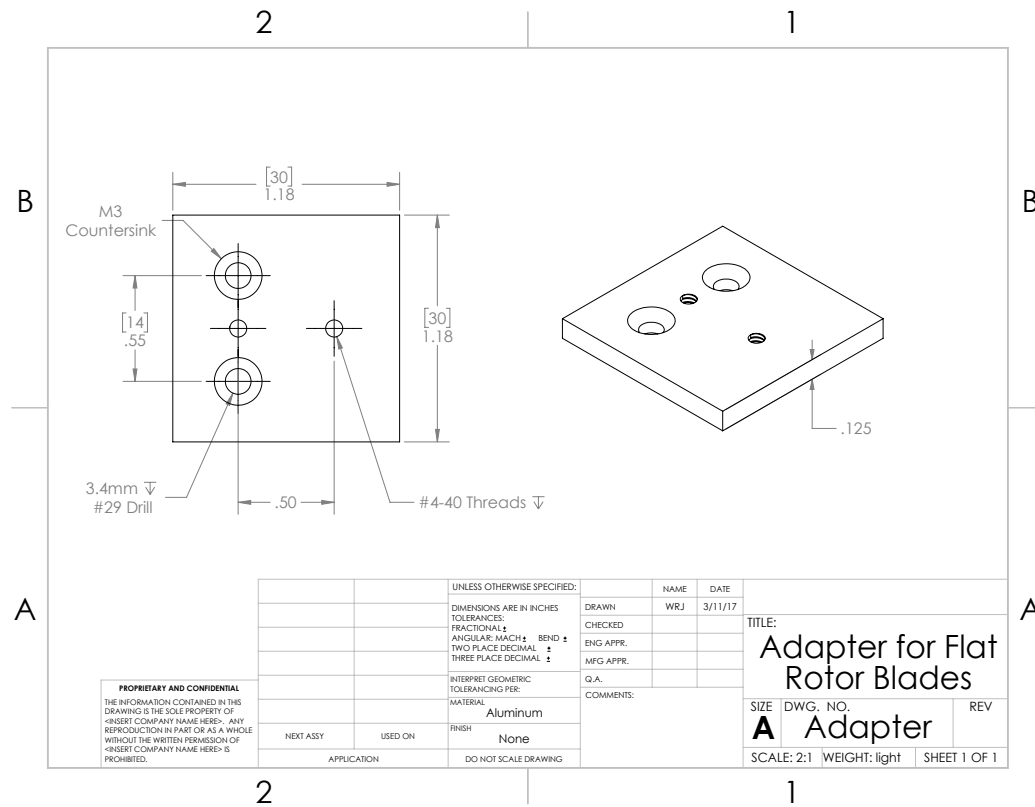


Figure 72: Adapter for using rectangular blades on wedges

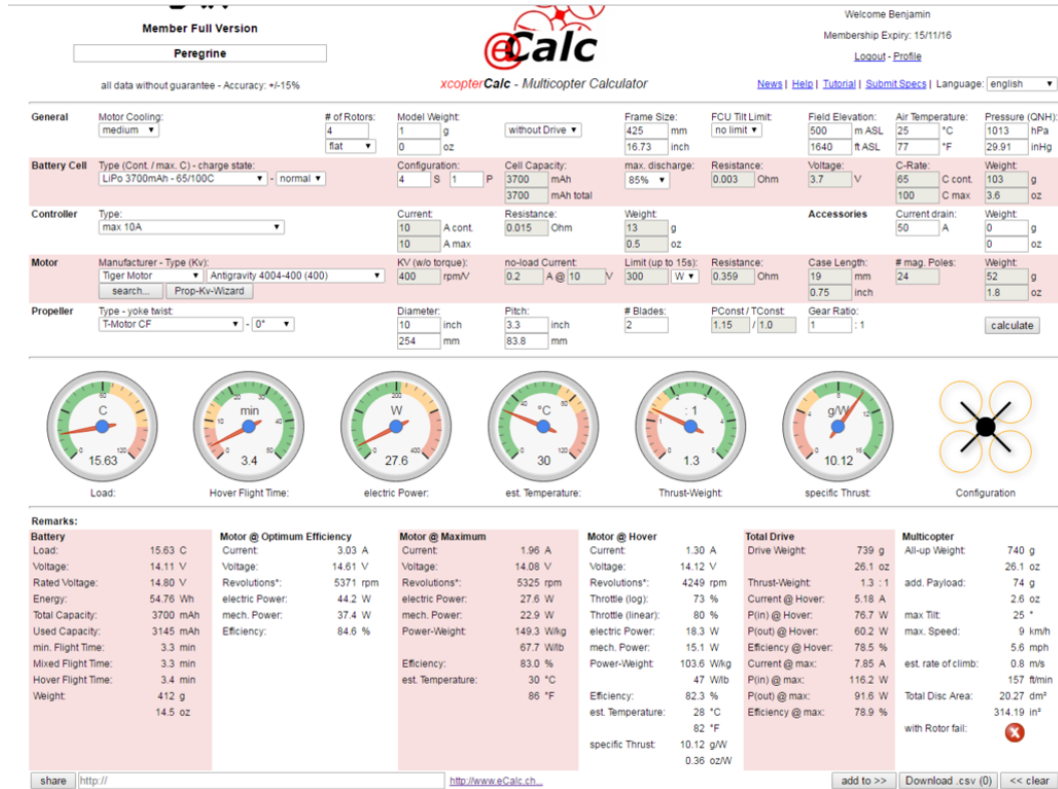


Figure 73: Quadrotor sizing results from eCalc.

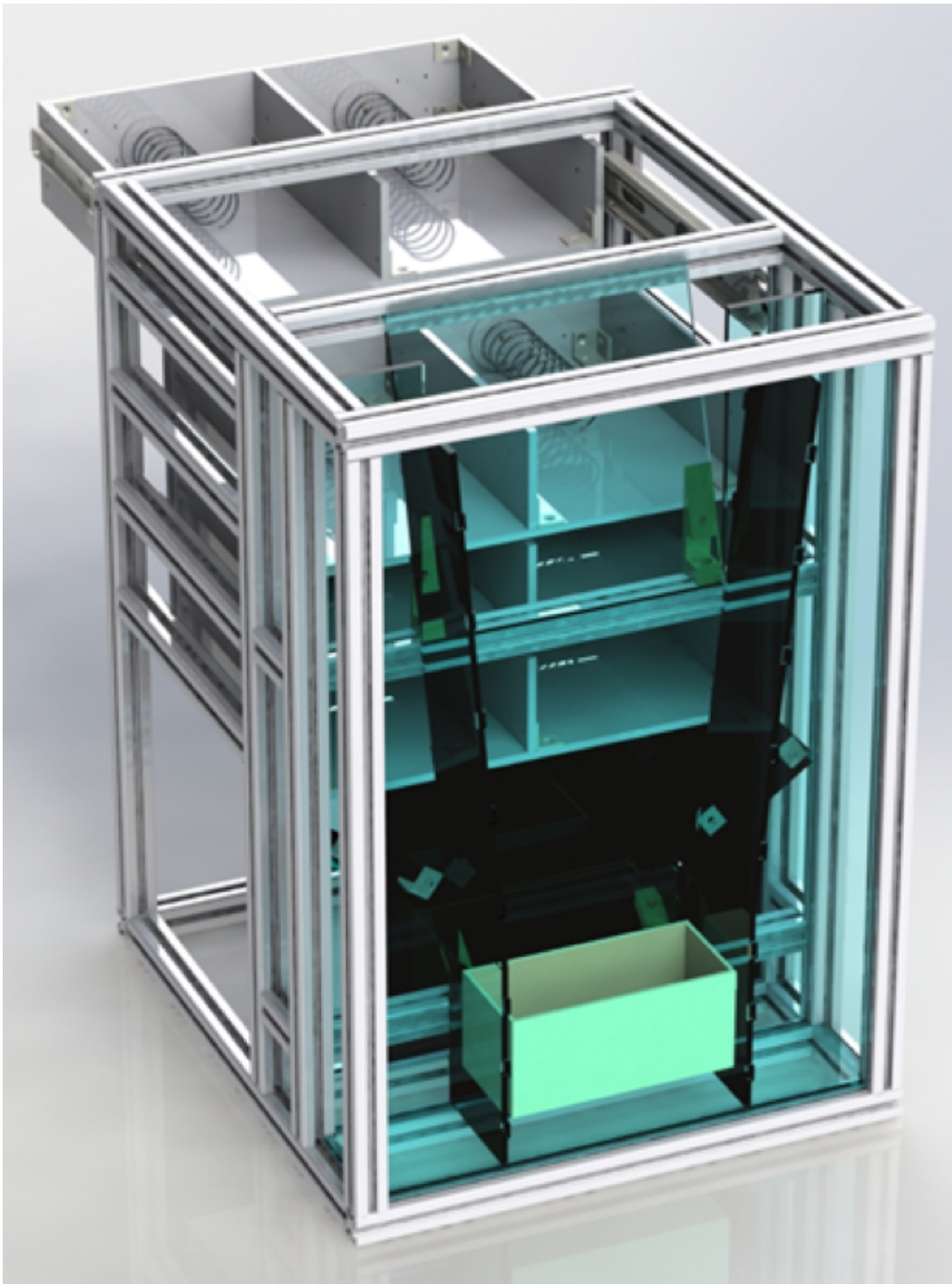


Figure 74: Final render of the custom vending machine

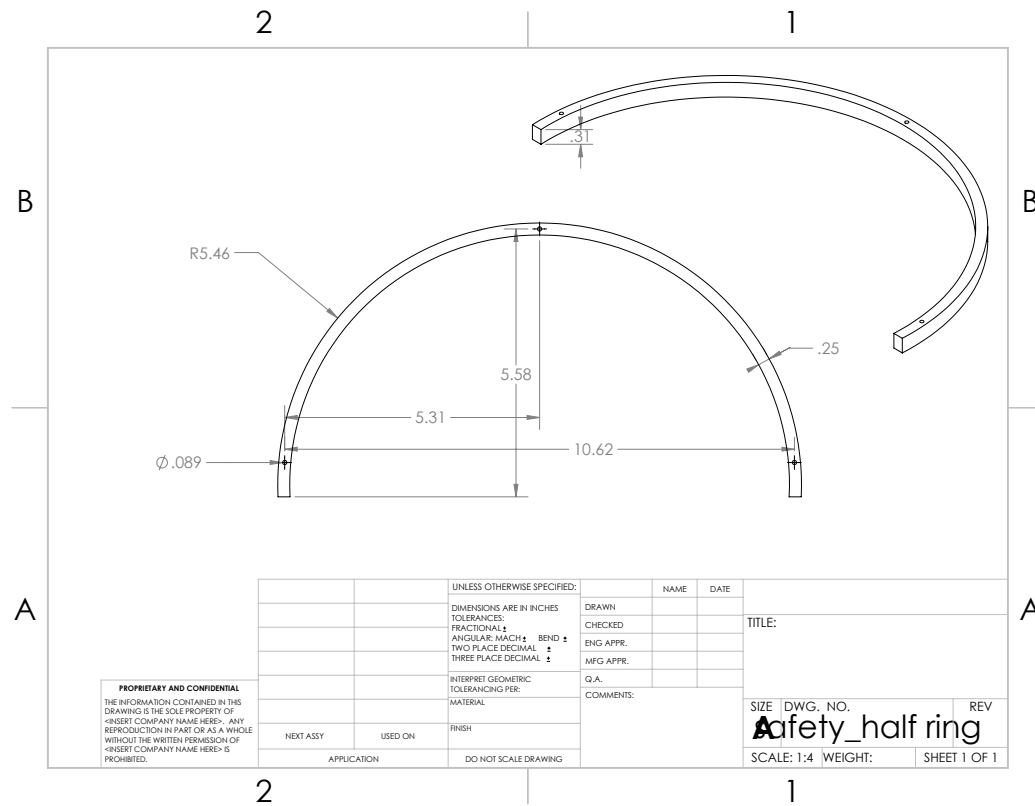


Figure 75: Quadrotor safety guards

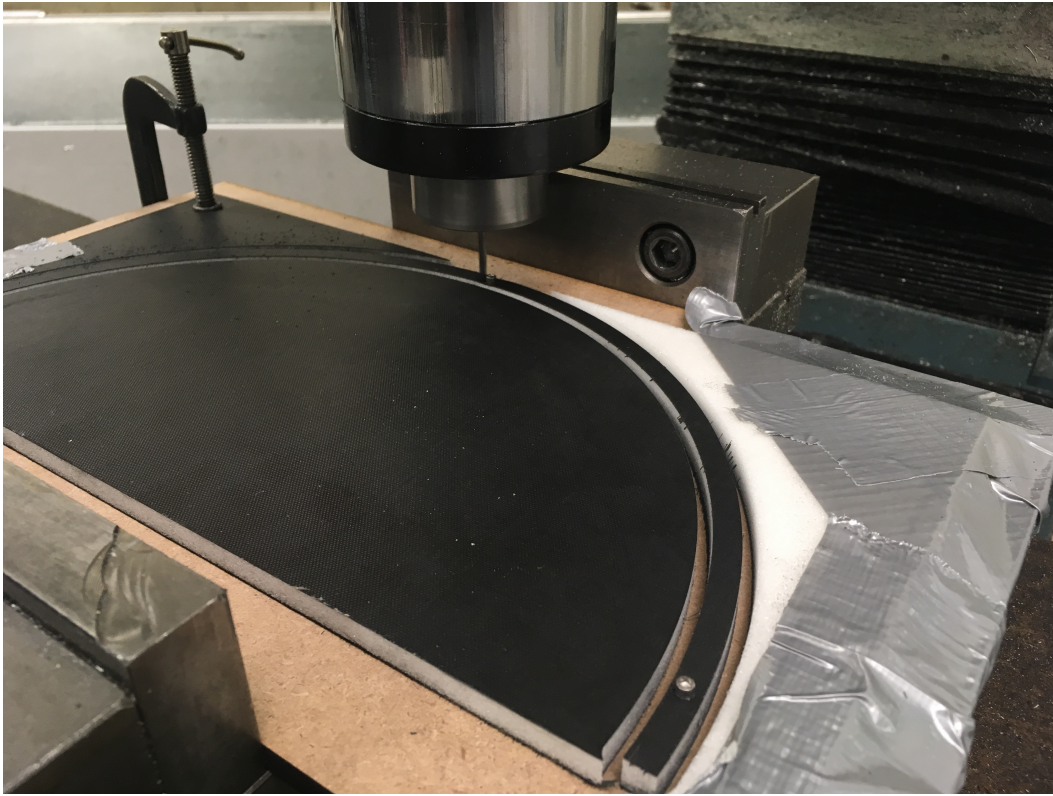


Figure 76: Machining the lower propeller safety guards

DragonPlate Carbon Fiber Foam Core Specifications: Upper Hoop ^a											
Foam Type	Thickness in	Weight lbs/ft ²	Weight of Hoop ^a lbs	Weight of 1 Hoop ^a g	Compressive Strength ^b psi	Compressive Modulus ^b psi	Shear Strength ^b psi	Shear Modulus ^b psi	Tensile Strength ^b	Tensile Modulus ^b	
Airex C70-40	0.5"	0.32	0.088	39.653	65	5370	65	1900	100	4060	
Airex C70-40	0.25"	0.48	0.081	36.602	65	5370	65	1900	100	4060	
Divinycell H100	0.5"	0.68	0.114	51.853	290	19580	232	5080	500	18855	
Divinycell H100	0.25"	0.61	0.103	46.516	290	19580	232	5080	500	18855	
*area of hoop = 24.24 in ²											
^b material properties are those of the core materials, which are weaker than the carbon fiber sandwich plates											
^c need 48"x48" panels to fit the parts, hence limited options											
Safety Support Rod Specifications											
Rod Material	OD in	ID in	Density lbs/in ³	Weight of 1 Lower Rod g	Weight of 1 Upper Rod g	Total Lower Rod Weight g	Total Upper Rod Weight g	Compressive Strength psi	Tensile Strength psi	Flexural Strength psi	Yield Strength psi
Carbon Fiber	0.188	0.116	0.06	2.456	5.520	20	22	75,000	120,000		89,000
Carbon Fiber	0.156	0.11	0.06	1.373	3.086	11	12	75,000	120,000		89,000
Carbon Fiber	0.254	0.158	0.06	4.439	9.975	36	40	75,000	120,000		89,000
Aluminum	0.24	0.152	0.1	6.452	14.500	52	58		30,000		35,000
Steel	0.188	0.118	0.283	11.339	25.480	91	102		58,000		70,000
Balsa	0.125	N/A	0.004	0.117	0.263	1	1	1,754	2,886		
*Length of Lower Rod: 5.26 Lower Rod Quantity: 8											
*Length of Upper Rod: 11.82 Upper Rod Quantity: 4											
Carbon Fiber Composite Specifications: Lower Hoop											
Composite Type	Thickness in	Weight lb/ft ²	Total Cost (for 4) \$	Weight of 1 Hoop ^a g	Compressive Strength ^b psi	Shear Strength ^b psi	Shear Modulus ^b psi	Tensile Strength ^b psi			
Rohacell Foam Core	0.25	0.287	\$74.40	4.44	317	189		4,205	600		
Airex C70-40	0.25	0.48	\$148	7.429	65	65	1900	100			
Divinycell H100	0.25	0.61	\$154	9.441	290	232	5080	500			
Balsa Core	0.25	0.68	\$165	10.525	1870	432	23100	1900			
*area of hoop: 4.92											
^b material properties are those of the core materials, which are weaker than the carbon fiber sandwich plates											

Figure 77: Safety material selection chart [63] [64] [66] [67] [65].

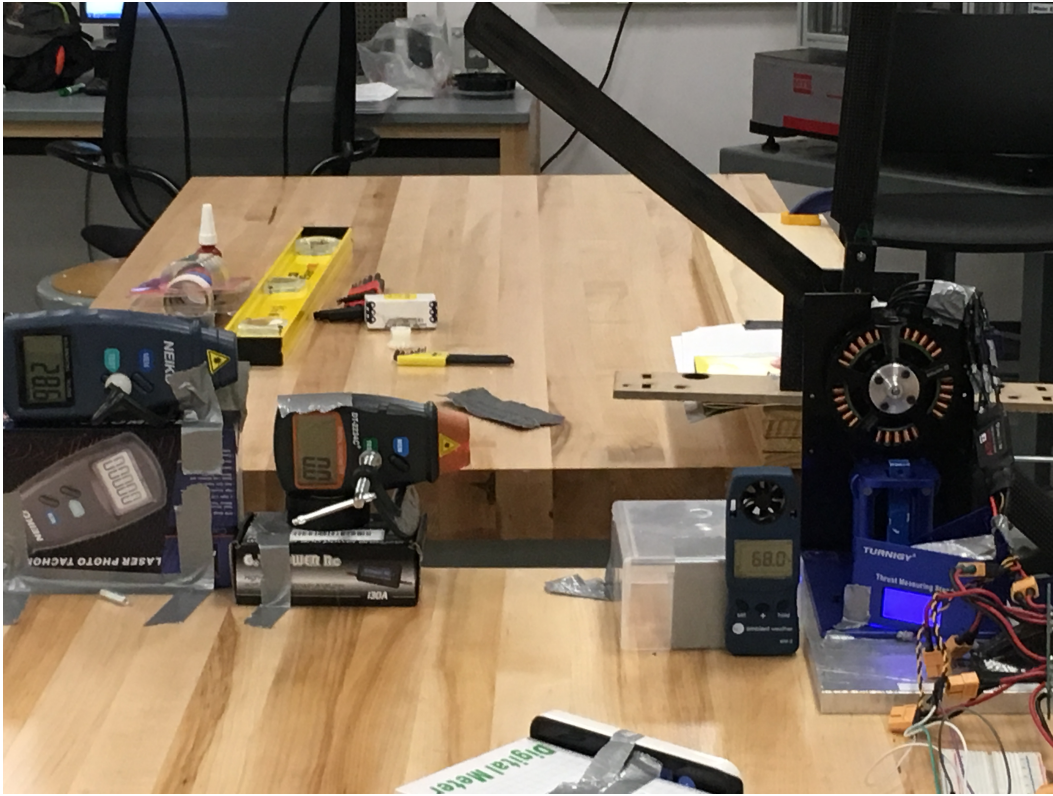


Figure 78: Aerodynamic test in B2



Figure 79: Preparing for a hover test in Moore 300

Table 12: Vehicle Mass Bill

Component	Quantity	Unit Mass (g)	
Carbon Fiber and Fiberglass Frame	1	571	
Antigravity 4004 Motor	4	57	
Propeller, 10x3.3	4	9	
Antigravity ESC	4	18	
U8 170Kv	2	245	
Propeller, 26x8.5	2	84	
U8 ESC	2	25	
Pixhawk Flight Controller	1	51	
Hokoyu URG-04LX LiDAR	1	139	
ODroid UX4	1	59	
Asus Xiton Pro, RGBD Camera	1	201	
LiPo 5S Battery	1	700	
Carriage & Motor	1	38	
Lower Safety Hoops, Rods, and Connectors	4	6	
Shelf	1	76	
Upper Shaft Collar and Adapter	1	64	
Lower Shaft Collar	1	25	
Plastic Wedges	2	18	
Wedge Adapter	1	56	
Landing Feet	4	37	
Electronics		200 Payload	300
Total		3,037	

Table 13: Vehicle Bill of Materials

Component	Quantity	Unit Mass (g)
Carbon Fiber and Fiberglass Frame	1	571
Antigravity 4004 Motor	4	57
Propeller, 10x3.3	4	9
Antigravity ESC	4	18
U8 170Kv	2	245
Propeller, 26x8.5	2	84
U8 ESC	2	25
Pixhawk Flight Controller	1	51
Hokoyu URG-04LX LiDAR	1	139
ODroid UX4	1	
Asus Xiton Pro, RGBD Camera	1	201
LiPo 5S Battery	1	700
Carriage & Motor	1	38
Lower Safety Hoops, Rods, and Connectors	4	6
Shelf	1	76
Upper Shaft Collar and Adapter	1	64
Lower Shaft Collar	1	25
Plastic Wedges	2	18
Wedge Adapter	1	N/A
Heat-set Threaded Inserts	8	
Rectangular Blade Adapter	2	17
Landing Feet	4	
Power Distribution Board	1	
Remote Kill Switch Board	1	
Assorted Fasteners	Not Specified	

Table 14: Vending and Dispensing Bill of Materials

Component	Quantity
8020	20 ft
8020 Connecting Plates	30
Fasteners	Not Specified
Drawer Slides	8
Corner Brackets	24
Acrylic Drawers	4
Stepper Motors	8
Arduino	1
Vending Machine Coil	8
Coil Adapters	8
Ramp and Chute	3 Sheets Acrylic
Candy	Not Specified

Table 15: Computer and Electronics Bill of Materials

Component	Quantity
Intel i3 CPU	1
Cool Master Evo 212	1
NVIDIA 1050 ti GPU	1
MSI Gaming H110 Motherboard	1
Kingston 120 GB SSD	1
Rosewill Micro-ATX Mini Tower Computer	1
8 GB RAM	1
EVGA 500 W1 Power Supply	1

References

- [1] Matthew Rocco. “Stadiums Struggle to Satisfy Hungry fans, Oracle Finds”. In: *Fox Business* (July 14, 2016). URL: <http://www.foxbusiness.com/features/2016/07/14/stadiums-struggle-to-satisfy-hungry-fans-oracle-finds.html> (visited on 10/24/2016).
- [2] Jenna McKnight. “Hollwich Kushner Creates University of Pennsylvania Incubator Space with Spiky Glass Facade”. In: *Dezeen* (Oct. 12, 2016). URL: <http://www.dezeen.com/2016/10/12/hollwich-kushner-pennovation-center-university-pennsylvania-incubator-space-spiky-glass-facade/> (visited on 10/26/2016).
- [3] Cameron Zawacki. *Empirical Data Collected at Sporting Event*. Madison Square Garden, Oct. 22, 2016.
- [4] Aethon. *TUG Smart Autonomous Mobile Robot*. Oct. 2013. URL: <http://www.aethon.com/wp-content/uploads/2013/10/TUGBrochureWeb.pdf> (visited on 10/24/2016).
- [5] Aethon. *Univeristy of Maryland Medical Center Case Study*. Aug. 2014. URL: <http://www.aethon.com/wp-content/uploads/2014/08/UMMC-Case-Study-2011b.pdf> (visited on 10/24/2015).
- [6] *The Future of Hotel Delivery Service*. In collab. with Savioke. Sept. 22, 2016. URL: <https://www.youtube.com/watch?v=b8IKfQLGIRQ> (visited on 10/23/2016).
- [7] Esther Hertzfeld. “Will robots ever replace guestroom minibars?” In: *Hotel Management* (Oct. 4, 2016). URL: <http://www.hotelmanagement.net/tech/will-robots-ever-replace-guestroom-minibars> (visited on 10/24/2016).
- [8] Bell and Howell. *Mailmobile 4: The Newest Generation*. 2002. URL: http://www.egeminusa.com/pdf/Egemin_Mailmobile4.pdf (visited on 10/23/2016).
- [9] Matt McFarland. “Drones delivering drinks in a crowded restaurant? It’s not as crazy as it sounds.” In: *The Washington Post* (Feb. 13, 2015). URL: <https://www.washingtonpost.com/news/innovations/wp/2015/02/13/drones-delivering-drinks-in-a-crowded-restaurant-its-not-as-crazy-as-it-sounds/> (visited on 10/23/2016).

- [10] Hyacinth Mascarenhas. “Festo’s bizarre bubble-like drone can swallow small objects for delivery with its chameleon-like tongue”. In: *International Business Times* (Apr. 13, 2016). URL: <http://www.ibtimes.co.uk/festos-bizarre-bubble-like-drone-can-swallow-small-objects-delivery-its-chameleon-like-tongue-1554583> (visited on 10/23/2106).
- [11] Amazon.com. *Amazon Prime Air*. 2017. URL: <https://www.amazon.com/Amazon-Prime-Air/b?node=8037720011> (visited on 04/20/2017).
- [12] Luke Johnson. *9 things you need to know about the Amazon Prime Air drone delivery service*. Feb. 7, 2011. URL: <http://www.digitalspy.com/tech/feature/a820748/amazon-prime-air-drone-delivery-service/> (visited on 04/20/2017).
- [13] April Glaser. *Watch Amazon’s Prime Air make its first public U.S. drone delivery*. Mar. 24, 2017. URL: <https://www.recode.net/2017/3/24/15054884/amazon-prime-air-public-us-drone-delivery> (visited on 04/20/2017).
- [14] William H. Blahd. *Harmful Noise Levels*. Nov. 14, 2014. URL: <http://www.webmd.com/brain/tc/harmful-noise-levels-topic-overview> (visited on 10/26/2016).
- [15] T-Motor. *T-Motor FPV Series Motors*. Oct. 2016. URL: http://www.rctigermotor.com/html/2016/fpvmotors_0407/307.html.
- [16] Scott Driessens and Paul E. I. Pounds. “Towards a more efficient quadrotor configuration”. In: IEEE, Nov. 2013, pp. 1386–1392. ISBN: 978-1-4673-6358-7 978-1-4673-6357-0. DOI: 10.1109/IR0S.2013.6696530. URL: <http://ieeexplore.ieee.org/document/6696530/> (visited on 10/23/2016).
- [17] Paul E. I. Pounds. “Towards the Stackrotor: Aerodynamics, Construction, Dynamics and Control of a Vertical Stacked-Rotor Configuration for Indoor Heavy-Lift Helicopter Robots”. In: *Unpublished* Unpublished.Unpublished (2016).
- [18] J. Gordan Leishman and Shreyas Ananthan. “Aerodynamic Optimization of a Coaxial Proprotor”. In: *Annual Forum Proceedings-American Helicopter Society* 62 (1 2006).
- [19] Johan Lozano. *Top Ten Best RC Helicopter -Guide and Review 2017*. URL: <http://rchelicop.com/>.
- [20] United States Access Board. *Chapter 4: Entrances, Doors, and Gates*. URL: <https://www.access-board.gov/guidelines-and-standards/buildings-and-sites/about-the-ada-standards/guide-to-the-ada-standards/chapter-4-entrances,-doors,-and-gates#ar2065> (visited on 04/01/2017).
- [21] Max Products International. *Himax Contrarotating Motors*. URL: <http://www.maxxprod.com/mpi/mpi-266.html>.
- [22] T-Motor. *U-8 Efficiency Type*. URL: http://www.rctigermotor.com/html/2013/Efficiency-Type_0928/94.html.
- [23] T-Motor. *U-10 Efficiency Type*. URL: http://www.rctigermotor.com/html/2014/Efficiency-Type_0314/198.html.
- [24] T-Motor. *U-12 Efficiency Type*. URL: http://www.rctigermotor.com/html/2016/Efficiency-Type_0106/306.html.
- [25] hobbyking.com. *ZIPPY Flightmax 8000mAh 4S1P 30C*. URL: https://hobbyking.com/en_us/zippy-flightmax-8000mah-4s1p-30c.html.

- [26] hobbyking.com. *MultiStar LiHV High Capacity 10000mAh 4S 10C Multi-Rotor Lipo Pack*. URL: https://hobbyking.com/en_us/multistar-lihv-high-capacity-4s-10000mah-multi-rotor-lipo-pack.html.
- [27] hobbyking.com. *Turnigy Graphene Professional 10000mAh 4S 15C LiPo Pack w/5.5mm Bullet Connector*. URL: https://hobbyking.com/en_us/turnigy-graphene-10000mah-4s-15c-w-5-5mm-bullet-connector.html.
- [28] hobbyking.com. *Multistar High Capacity 16000mAh 4S 10C Multi-Rotor Lipo Pack*. URL: https://hobbyking.com/en_us/multistar-high-capacity-4s-16000mah-multi-rotor-lipo-pack.html.
- [29] T-Motor. *G26x8.5prop-4PCS/PAIR*. URL: http://www.rctigermotor.com/html/2013/prop_0805/10.html.
- [30] Horizon Hobby. *325mm Carbon Fiber Main Rotor Blade Set B400*. URL: <https://www.horizonhobby.com/325mm-carbon-fiber-main-rotor-blade-set\%3A-b400-eflh1415c>.
- [31] xheli.com. *CNC Metal Complete Rotor Head*. URL: <http://www.xheli.com/cncmecorohe1.html>.
- [32] Hobbyking.com. *Turnigy nano-tech 5000mah 5S 25 50C Lipo Pack*. URL: https://hobbyking.com/en_us/turnigy-nano-tech-5000mah-5s-25-50c-lipo-pack.html.
- [33] Markus Müller. *eCalc - the most reliable RC Calculator on the Web*. Oct. 2016. URL: ecalculator.ch.
- [34] Amazon. *Intel NUC NUC5i5RYH*. URL: <https://goo.gl/ndX81q>.
- [35] Amazon. *Intel NUC Kit NUC5i7RYH*. URL: <https://goo.gl/PqbB7m>.
- [36] KITTI. *Visual Odometry / SLAM Evaluation 2012*. URL: <https://goo.gl/mPjKCy>.
- [37] Bodin B. Zia M. Z. Mawer J. Nisbet A. Kelly P. H. J. Davison A. J. Lujan M. O'Boyle M. F. P. Riley G. Topham N. Furber S. Nardi L. "Introducing SLAMBench, a performance and accuracy benchmarking methodology for SLAM". In: *IEEE Xplore* (2015).
- [38] Hokuyo. *URG04-LX*. URL: <https://goo.gl/rFLPv1>.
- [39] RobotShop. *Hokuyo URG-04LX Scanning Laser Rangefinder*. URL: <https://goo.gl/cJFy13>.
- [40] Hokuyo. *URG-04LX-F01*. URL: <https://goo.gl/lpkXrk>.
- [41] Hokuyo. *Hokuyo URG-04LX-F01 (Rapid URG) Scanning Laser Rangefinder*. URL: <https://goo.gl/UxmCJO>.
- [42] Hokuyo. *URG04-LX-UG01*. URL: <https://goo.gl/CQH5ie>.
- [43] RobotShop. *Hokuyo URG-04LX-UG01 Scanning Laser Rangefinder*. URL: <https://goo.gl/9xLk0u>.
- [44] Hokuyo. *UTM30-LX*. URL: <https://goo.gl/RfHRFF>.
- [45] RobotShop. *Hokuyo UTM-30LX Scanning Laser Rangefinder*. URL: <https://goo.gl/8761Cu>.
- [46] RobotShop. *RPLiDAR A2*. URL: <https://goo.gl/Jq3iWm>.

- [47] Velodyne. *Velodyne LiDAR Puck LITE: Light Weight Real-Time 3D LiDAR Sensor*. Electronic.
- [48] Sean Higgins. *Velodyne Announces \$7,999 PUCK LiDAR Sensor*. Aug. 2014. URL: <https://goo.gl/AeKXXY>.
- [49] SICK. *2D Laser Scanners TiM5xx/ TiM51x/Indoor*. URL: <https://goo.gl/xrGZwy>.
- [50] PLC Center. *TIM510-9950000S01*. URL: <https://goo.gl/vMrCHw>.
- [51] HardKernel. *Odroid-XU4 [ODroid-XU4]*. URL: <https://goo.gl/RHryZ5>.
- [52] HardKernel. *ODroid XU4*. URL: <https://goo.gl/AYm9OR>.
- [53] Raspberry Pi. *Raspberry Pi 3 Model B*. URL: <https://www.raspberrypi.org/products/raspberry-pi-3-model-b/>.
- [54] Amazon. *Rapsberry Pi 3 Model B Motherboard*. URL: <price:https://goo.gl/aavNhq>.
- [55] BeagleBoard. *BeagleBone Black*. URL: <https://goo.gl/9cPiZS>.
- [56] Amazon. *Beagleboard (BeagleBone Rev C)*. URL: <https://goo.gl/U6b8VA>.
- [57] Gumstix. *Overo Firestorm-Y Technical Specifications*. URL: <https://goo.gl/nBsbWb>.
- [58] Gumstix. *Overo Firestorm-Y COM*. URL: <https://goo.gl/h0W2mp>.
- [59] Gumstix. *Duovero Zephyr-Y Technical Specifications*. URL: <https://goo.gl/r60o6m>.
- [60] Gumstix. *Duovero Zephyr-Y COM*. URL: <https://goo.gl/cXeBVU>.
- [61] NVidia. *Unleash Your Potential with the Jetson TX1 Development Kit*. URL: <https://goo.gl/cmPC4g>.
- [62] NVidia. *NVidia Jetson TX1 System-On-Module*. Online.
- [63] DragonPlate. URL: <https://dragonplate.com/>.
- [64] Evonik Industries AG. *Technical Information: ROHACELL IG/IG-F*. Jan. 2014. URL: <https://www.rockwestcomposites.com/media/wysiwyg/ROHACELL-IG-IG-F-mechanical-properties-EN.pdf>.
- [65] McMaster-Carr. *Carbon Fiber Tubes*. URL: <https://www.mcmaster.com/#carbon-fiber-tubing/=17eblef>.
- [66] *Balsa wood Properties Guide*. URL: <http://www.auszac.com/Balsa\%20wood\%20Properties\%20Guide.pdf>.
- [67] The Wood Database. *Balsa*. URL: <http://www.wood-database.com/balsa/>.
- [68] *TCF BANK STADIUM CONCOURSE*. 2009. URL: <https://www.flickr.com/photos/28719853@N03/3848874268>.
- [69] *7 Hours in Terminal B*. Apr. 2016. URL: <http://annrasmussenwriter.com/2016/01/04/7-hours-in-terminal-b/>.
- [70] Suntec Singapore. URL: <https://www.suntecsingapore.com/>.
- [71] Level Group. *Manufacturing*. URL: <http://levelgrouppltd.com/manufacturing/>.